POLITECNICO
MILANO 1863

SCUOLA DI INGEGNERIA INDUSTRIALE
E DELL'INFORMAZIONE

Control Tuning of Autonomous Vehicles Considering Performance-Comfort Trade-offs

Tesi di Laurea Magistrale in
Automation and Control Engineering

Author: **Kimia Mesghali**

Student ID: 10721013
Advisor: Prof. Lorenzo Mario Fagiano
Academic Year: 2021-2022

Abstract

A wide range of studies and companies are focusing on autonomous vehicles these days. They strive to provide vehicles that are safe and reliable. Safety and reliability play a crucial role in the acceptance of self-driving cars by customers. In addition, passenger comfort is another crucial aspect that affects the acceptance of autonomous vehicles. In order for autonomous vehicles to follow the road, different aspects such as perception, path planning, and control can be studied. The control part of autonomous vehicles is vital to ensuring passenger's comfort.

This thesis focuses on the development of control systems for autonomous vehicles that consider comfort-performance trade-offs. Vehicles are considered in a static environment, and roads are predefined. In the first step, the mathematical model of the vehicle is adopted, then the longitudinal and lateral controllers for the vehicle are developed. The controllers for the vehicle are developed in such a way as to ensure the comfort of passengers.

Initially, the lateral controller has a cascade loop design and uses Frenet-Serret formula in conjunction with the Linear Quadratic Regulator (LQR) approach to design the outer loop, and a yaw rate controller in the inner loop. After that, the longitudinal controller is developed, which is composed of reference speed generation and cruise controller.

Several key parameters of the controllers were then optimized using the Gridding approach in favor of passenger comfort and vehicle performance. Considering that these objectives conflict, a multi-objective analysis is performed to find the Pareto Front and then the appropriate solution. In addition, To evaluate the performance of the closed-loop system, real-world roads are tested. Simulink and MATLAB were used to implement the whole system.

Keywords: Autonomous vehicles, comfort , path-following, lateral control, longitudinal control, multi-objective optimization

Abstract in lingua italiana

Una vasta gamma di studi e aziende si sta concentrando sui veicoli autonomi in questi giorni. Si sforzano di fornire veicoli sicuri e affidabili. La sicurezza e l'affidabilità giocano un ruolo cruciale nell'accettazione delle auto a guida autonoma da parte dei clienti. Inoltre, il comfort dei passeggeri è un altro aspetto cruciale che influisce sull'accettazione dei veicoli autonomi. Affinché i veicoli autonomi seguano la strada, è possibile studiare diversi aspetti come la percezione, la pianificazione del percorso e il controllo. La parte di controllo dei veicoli autonomi è vitale per garantire il comfort dei passeggeri.

Questa tesi si concentra sullo sviluppo di sistemi di controllo per veicoli autonomi che considerano i compromessi comfort-prestazioni. I veicoli sono considerati in un ambiente statico e le strade sono predefinite. Nella prima fase viene adottato il modello matematico del veicolo, quindi vengono sviluppati i controller longitudinali e laterali per il veicolo. I controller per il veicolo sono sviluppati in modo tale da garantire il comfort dei passeggeri.

Inizialmente, il controller laterale ha un design ad anello in cascata e utilizza la formula Frenet-Serret in combinazione con l'approccio del regolatore quadratico lineare (LQR) per progettare l'anello esterno, e un controller della velocità di imbardata nell'anello interno. Successivamente, viene sviluppato il controller longitudinale, composto dalla generazione della velocità di riferimento e dal regolatore di velocità.

Diversi parametri chiave dei controller sono stati quindi ottimizzati utilizzando l'approccio Gridding a favore del comfort dei passeggeri e delle prestazioni del veicolo. Considerando che questi obiettivi sono in conflitto, viene eseguita un'analisi multi-obiettivo per trovare il fronte di Pareto e quindi la soluzione appropriata. Inoltre, per valutare le prestazioni del sistema a circuito chiuso, vengono testate strade del mondo reale. Simulink e MATLAB sono stati utilizzati per implementare l'intero sistema.

Parole chiave: Veicoli autonomi, comfort, inseguimento del percorso, controllo laterale, controllo longitudinale, approccio multiobiettivo

Contents

Introduction

The idea of autonomous vehicles has been around for decades. However, drastic improvements in the automotive field in the last decade have turned this idea into reality.

In 2004, DARPA held a competition in autonomous vehicle racing while none of the self-driving cars completed the route. One year after, five driverless cars managed to navigate the whole path. In 2014, Google's self-driving car drove over 700,000 miles on California public roads. In addition, many big companies like BMW, Volvo, Audi, and Toyota have embarked on the world of autonomous vehicles since 2010 [11].
The impacts of self-driving cars are not negligible. Firstly, safety will significantly improve. As, around 40% of fatal accidents are due to human mistakes like alcohol, distraction, and fatigue. However, AVs are not affected by human failings resulting in at least a 40% reduction in fatal accidents. Another beneficial impact is on road congestion. AVs can estimate leading cars' speeds and accelerations and adopt fine speed adjustment and braking that can result in fewer congestions and lower fuel consumption. In addition, AVs can facilitate juniors, elderlies, and disabled people to travel [11].

Although AVs provide many benefits, there are challenges and barriers in this industry. Firstly, the cost of self-driving cars is high due to the additional sensors and guidance technology. As it transforms from the test phase to mass production, the costs can slightly drop but still remains high. The other barrier is legislation and certification. Self-driving cars are just allowed in some states in the U.S with severe limitations. New safety rules and laws should be provided for these new vehicles.

Safety and comfort of passengers have been the body of researches over the past years. In fact, there is a strong correlation between the comfort and acceptance of autonomous vehicles. Many different definitions of comfort have been provided in the literature. However, there is no clear unit definition for it. The comfort definition is subjective and influenced by many external environmental factors like noise, light, and temperature [28].

Studies have shown that acceleration and deceleration, as well as their temporal derivatives, jerk, significantly affect passenger comfort. Therefore, one of the ways to provide comfort for passengers is to keep these parameters within particular thresholds. The

self-driving car can reach this goal by applying adequate longitudinal and lateral control.

In this thesis, the aim is to provide a comfortable driving experience for passengers. Therefore, during path following and planning, three aspects were taken into account. Firstly, passengers' comfort as acceleration and jerk minimization. Additionally, time optimization is needed to make the autonomous vehicle as fast as possible. Moreover, the vehicle has been kept within the limits of realistic real-world lanes during path-following. To achieve all these goals together, a multi-objective optimization strategy has been used. Furthermore, due to models of vehicles and controllers, the problem is highly nonlinear and non-convex. Thus, first a proper lateral and longitudinal control of the autonomous vehicle is designed and then the closed-loop system parameters are optimized to reach the desired goals.

The contributions of the thesis can be listed as follows:

- The vehicle model appropriate for our goal of designing lateral and longitudinal controllers is taken from the literature in chapter 2. Next, a method is presented for defining a reference path as well as extracting the features needed for trajectory planning and path-following.
- The vehicle's driver has two tasks. Firstly, the driver is responsible for controlling the speed and braking. As well, the driver should follow the desired path by adjusting the steering of the vehicle. Therefore, the driver can act as a controller of the system while the vehicle is the plant of the system. These two components make up the whole closed-loop system. In chapter 3 the design of lateral and longitudinal controllers is described. The designs of the two controllers are geared toward passenger comfort. The driver model consists of two parts: high-level controllers and low-level controllers. We design the desired yaw rate and speed considering comfort in the high-level controllers, while in the low-level controllers, inputs of the vehicle is modified to meet the desired reference points.
- In chapter 4, an optimization algorithm is employed to tune the selected control parameters based on the comfort-performance of autonomous vehicles. Then, a multi-objective analysis is performed to determine the Pareto front. Finally, the tuned controllers are applied to real-world roads for evaluation.

In addition, there exist various path-following approaches for autonomous vehicles. Some of them are not practical due to their complexity, reliability, while others are more effective depending on the intended use. Various path following strategies from literature are discussed in chapter 1, along with comfort definitions while driving autonomous vehicles.

1 | Literature Review

1.1. Path-following

The objective of path following is to follow the pre-defined path by commanding the control inputs to the vehicle. Therefore, the position of the vehicle is needed at each time. This position should be compared to pre-defined path information and the control inputs should be adjusted based on error. Radars, gyroscopes, accelerometers, and cameras can be used to estimate a vehicle's position[27]. Moreover, in some cases, paths should be planned from a starting point to a target point considering the constraints of the road and vehicle. Clothoid arcs and Bézier curves [34] have been widely used to generate the path for autonomous systems. While planning the trajectory with the help of these curves, the rate of steering should be taken into consideration. Sudden changes of steering angles result in discomfort and instability of the lateral motion.
Though the lateral motion and longitudinal motion of the vehicle are highly coupled, most articles just focus on lateral control to follow the desired path while considering a constant speed for the vehicle.

1.1.1. Geometric Path-following

Among different path-following strategies, geometric ones are popular. Geometric following techniques utilize the geometric relationship between path and vehicle to generate control commands. Moreover, they use the look-ahead distance to measure the error between the car and the path.
Pure pursuit is one of the common geometrical methods [4]. The core idea of this method is that the target point can be placed on the path at a fixed distance from the vehicle and the steering command should bring the vehicle toward the path considering the target point. To construct Pure Pursuit law, we use the concept of instantaneous center of rotation. The target point on the path, the center point on the rear axle, and the instantaneous center of rotation form a triangle (see figure 1.1).

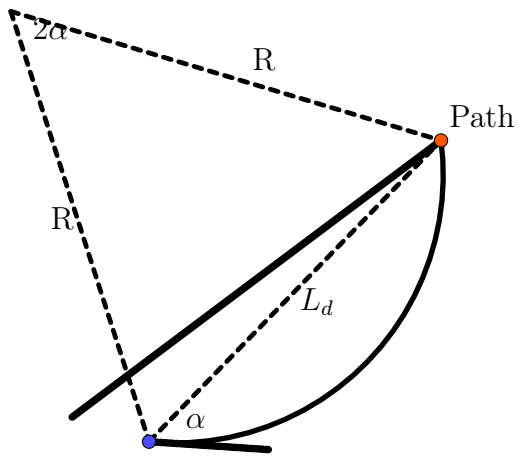

Figure 1.1: Pure Pursuit Geometry

based on law of sines, we can write the following equation:

$$\frac{L_d}{\sin 2w} = \frac{R}{\sin(\frac{\pi}{2} - w)} \tag{1.1}$$

Cross-track error is shown in figure 1.2.

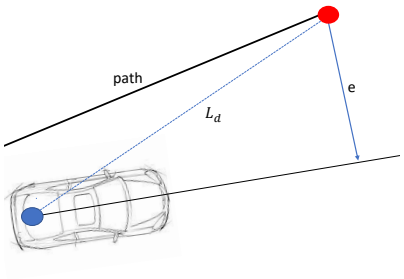

Figure 1.2: Cross-track Error

Finally, the pure pursuit control law can be written as:

$$\delta = arctan(\frac{2L\sin\alpha}{KV_x}) \tag{1.2}$$

Where K is the gain of control law and V_x is the longitudinal velocity of the vehicle. L is the length of vehicle and α has been shown in figure (1.1).
Stanely is another famous geometric lateral controller [32]. This approach has been developed by Stanford University's Darpa Grand challenge autonomous vehicle team. The

reference point on the vehicle is different than Pure Pursuit. This is on the center of the front axle. This updated reference point can result in better control and global convergence to the path. Furthermore, the error is computed both on heading angle and the position of the vehicle relative to the closest point on the path. Additionally, Stanely captures the steering angle if it falls between the thresholds.
Firstly, the controller attempts to align the vehicle to the desired path by setting the steering angle to the heading angle error which is the error between heading angle of vehicle and tangent angle of path.

$$\theta_e = \theta_{path} - \theta_{vehicle} \tag{1.3}$$

Then the second adjustment is applied based on the position error which is the error between the center of the front axle and the nearest point on the path.Therefore, the final steering control law is:

$$\delta = \theta_e + \arctan(\frac{ke_a}{V_x}) \tag{1.4}$$

Where k is a gain parameter. As the error increases, higher value of steering angle directs vehicle to the path. The errors are shown in figure (1.3).

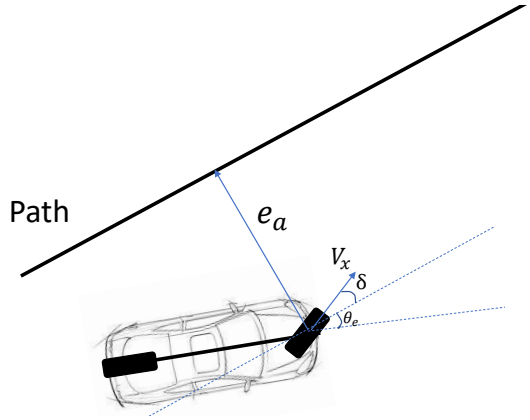

Figure 1.3: Stanely Geometric

1.1.2. Path-following Using Kinematic Model

Other than geometric path following controllers, there are many ways to track a trajectory based on the kinematic model of a vehicle. A common approach to robot motion planning is to simplify the vehicle system model to a kinematic bicycle model, simple vehicle model obtaining straightforward control laws. A solution to path following is provided according to the kinematic model of the vehicle.

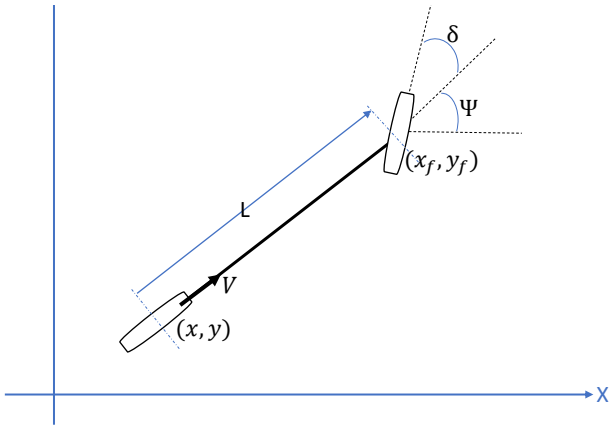

Figure 1.4: Kinematic model of vehicle

Equations of motion for the kinematic bicycle model can be found in [21]. In addition, feedback controllers designed for this model to follow the trajectory are available in [21]. Neglecting the dynamics of a vehicle can have a negative impact on path following. The vehicle's kinematic model has inaccurate results at high speeds. Furthermore, the kinematic model can fail on paths where curvatures change rapidly.
In this thesis, the dynamic model of the vehicle is used for path following which will be discussed in section (2.1).

1.2. Comfort in Autonomous Vehicles During Path-following

Comfort of passengers is a subjective definition and can be affected by many factors although many ways are provided in the literature to measure it. Several types of features can affect passengers' comfort: dynamic factors like acceleration, vibration, and shock. Ambient factors, such as thermal comfort, air quality, noise, pressure gradients, and spatial elements like the ergonomics of the passenger's position [7]. In [8], ambient factors are taken into account and different measurement indexes are provided based on them. However, in this thesis, comfort has been considered when it comes to dynamic characteristics.
As seen in the figure (1.5), passengers are imposed by three forces while seated in the car. The forces related to road disturbances can be reduced by proper seat designs. In addition, longitudinal forces are the result of acceleration/braking, and lateral forces come from steering [10].

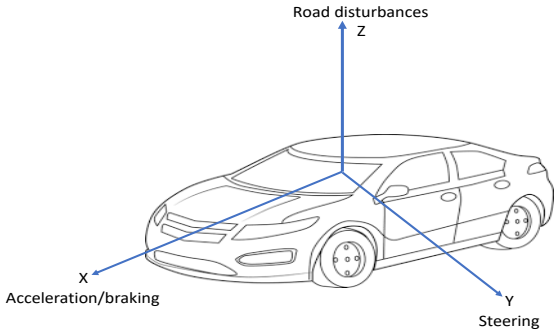

Figure 1.5: Forces acting on passenger

Towards passenger comfort, the most common approach is to minimize the forces and jerk acting on the passenger. Jerk is the third derivative of the position with respect to time. Jerk is felt due to the change in force. Comfort can be maximized by minimizing longitudinal and lateral acceleration and jerks [20], [25]. Motion sickness is another index to measure passengers' comfort. A person suffers from motion sickness when a conflict between their vestibular and visual senses happens. For example, reading in a car increases your chances of feeling motion sick since the standing field of view conflicts with the vestibular system's perception of vehicle acceleration [6].
Motion sickness can be measured numerically in many ways. Some models are based on vertical acceleration while others take longitudinal and lateral acceleration into account. First, the model developed in human factors research [23] which is based on the value, frequency and duration of vertical acceleration. The HFR model consists of a standardized normal distribution function for two variables: vertical harmonic oscillation with amplitude z_a and vertical frequency f during its exposure time, z_t'. This model is described by the following equation.

$$MSI = 100.\Phi(z_a).\phi(z_t') \tag{1.5}$$

$$\phi(z) = \frac{1}{2\pi}\int_{-\infty}^{z} e^{-\frac{1}{2}x^2}dx \tag{1.6}$$

HFR's disadvantages include its complexity and limitation to vertical accelerations.
Another MS model based on vertical acceleration can be found in [17], a standard for predicting vomiting (VI) and illness rating (IR). The developed model contains a cumulative measure of motion sickness, which is determined by the Motion Sickness Dose Value

(MSDV).

$$MSDV_z = \sqrt{\int_0^T a_v^2(t)dt} = a_{rms,v}\sqrt{T} \tag{1.7}$$

where T is the total time of driving , and a_v vertical acceleration. Motion Sickness Dose Value can also be used to predict vomiting (VI) and illness rating (IR) as following:

$$VI = K_m * MSDV \tag{1.8}$$

$$IR = K_r * MSDV \tag{1.9}$$

Where $K_r = 0.02$ and $k_m = 0.333$.
The Lawther and Griffin's model can also be extended to lateral and longitudinal accelerations which will be discussed in section (4.1).
Another way to ensure passengers' comfort is to keep accelerations and jerks within predetermined limits. Acceleration and jerks higher than these thresholds result in the discomfort of passengers. In [12], [26], [31] different restrictions are applied to acceleration and jerk while ensuring a comfortable driving experience. In [26], three modes are defined based on acceleration.

	Acceleration(m/s^2)	**Comfort**
Mode 0	-2<a<2	comfortable
Mode 1	-4<a<-2 or 2<a<4	uncomfortable
Mode 2	a<-4 or a>4	dangerous situation

Table 1.1: Different comfort levels based on acceleration

The limits used in this thesis will be elaborated in section (4.1).

2 | Path and Vehicle Model

First of all, we have to provide a mathematical model of the vehicle to understand how the vehicle reacts in the environment. Therefore, we can have a better understanding of the interaction between vehicles and paths. We can then design a path-following strategy based on this understanding. The model of the vehicle and the path are both required. There are many ways to model vehicles in the literature. The dynamic bicycle model was selected as kinematic models may fail at high speeds. In addition, bicycle models are less complex, but also represent a complete model of the vehicle.
Moreover, The model of the reference path is also another thing to consider. The characteristics of the path are drawn from them and used for path-following purposes. In this thesis, the paths are static and predefined. This means that all their features are known and used for path following.

2.1. Vehicle Model

Several methods can be used to model a vehicle, including geometries, kinematics, and dynamics. In this section, dynamic non-linear and linear bicycle model of vehicle is provided. In this thesis, path following algorithm and controllers are designed using these two models.

2.1.1. Non-linear Bicycle Model

The term bicycle model refers to the fact that both the front wheels of vehicle are taken as a single unit, and also both the rear wheels are taken as one, making it a two wheel model. Six-degree-of-freedom bicycle model of the vehicle is discussed. [2]
There are two frames then: Inertial frame which is attached to the vehicle and the global frame X_axis and Y_axis. Longitudinal and lateral positions of the vehicle (X, Y) are in relation to the global frame. Yaw angle (ψ) is the angle between inertial x_axis and global X_axis. Vehicle velocity (V), and its projection on internal coordinates are V_x and V_y. The angle between V and V_x is defined as the side slip angle(β), and yaw rate which is denoted as r (see figure 2.1).

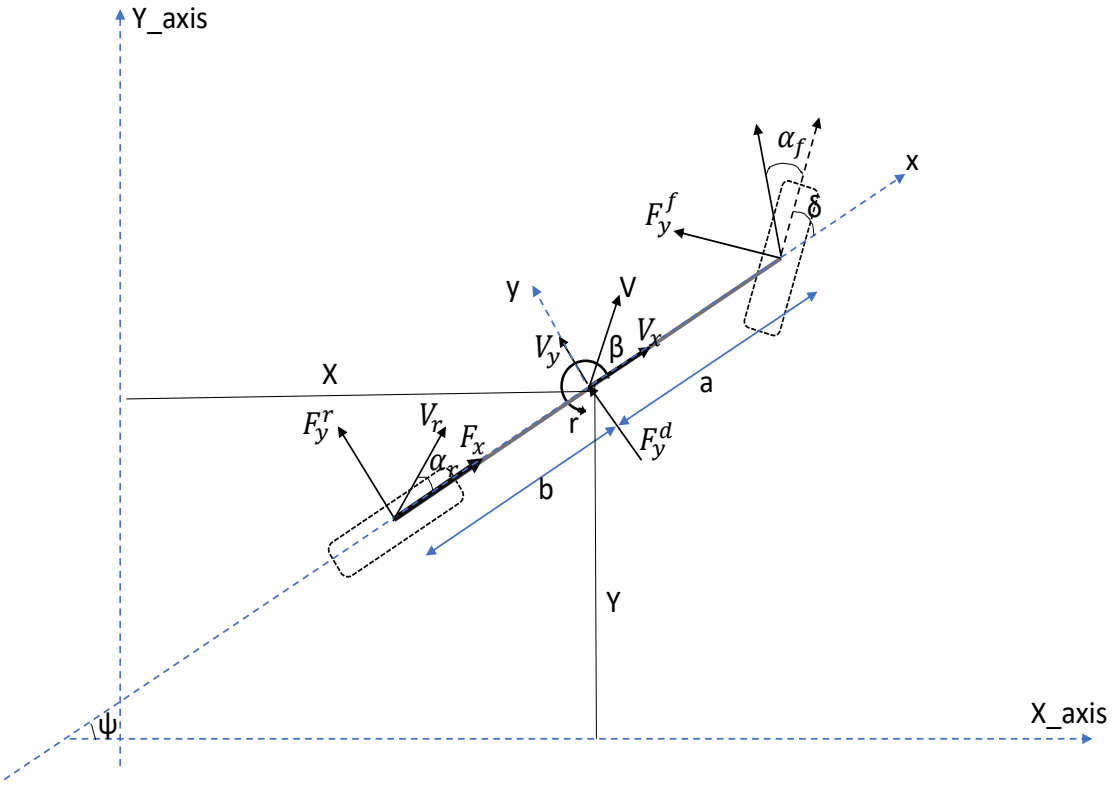

Figure 2.1: Dynamic bicycle model of vehicle

Therefore:

$$V_y = \tan(\beta)V_x \tag{2.1}$$

Applying Newton's second law for motion along the inertial y_axis:

$$ma_y = F_y^f + F_y^r \tag{2.2}$$

Where a_y is the the inertial acceleration of vehicle along y_axis and F_y^f, F_y^r are the lateral forces of the front and rear tire respectively.
Then, lateral forces should be modeled. For small slip-angles, the lateral tire force of a tire is proportional to the slip-angle. A tire's slip angle is defined as the angle between the tire's orientation and the wheel's velocity vector orientation. α_r and α_f in figure (2.1). There is a physical explanation for why the lateral tire force is proportional to the slip

angle in [29]. The slip angles can be defined as follows:

$$w_f = \arctan(\frac{V_y + ar}{V_x}) - \delta \tag{2.3}$$

$$w_r = \arctan(\frac{V_y - br}{V_x}) \tag{2.4}$$

Where r is the yaw rate of vehicle. δ is the front steering angle, a and b are the distance from front and rear axle of vehicle to COG respectively. (see figure 2.1)
It is not valid to assume that the lateral tire force is proportional to the slip angle at large slip angles. As a result, the lateral tire force will be affected by slip angle, the normal tire load (F_z^f, F_z^r.), the tire-road friction coefficient(μ). For simplicity, F_z^f and F_z^r are taken as constants and are written as follows:

$$F_z^f = mg\frac{b}{a+b} \tag{2.5}$$

$$F_z^r = mg\frac{a}{a+b} \tag{2.6}$$

Where m is the total mass of the vehicle, and g is the acceleration due to gravity. Finally, the lateral forces can be modeled as:

$$F_y^f = \min\left(\mu F_z^f, \max(-\mu F_z^f, -C_f z_f + \frac{C_f^2|z_f|z_f}{3\mu F_z^f} - \frac{C_f^3 z_f^3}{27\mu^2(F_z^f)^2})\right) \tag{2.7}$$

$$F_y^r = \min\left(\mu F_z^r, \max(-\mu F_z^r, -C_r z_r + \frac{C_r^2|z_r|z_r}{3\mu F_z^r} - \frac{C_r^3 z_r^3}{27\mu^2(F_z^r)^2})\right) \tag{2.8}$$

Where, $z_f = \tan\alpha_f$ and $z_r = \tan\alpha_r$ and C_r and C_f are the corning stiffness of the rear and front tire.
Moment balance about the z axis results in the equation for the yaw dynamics as:

$$J_Z\ddot{\psi} = aF_y^f\cos(\delta) - bF_y^r \tag{2.9}$$

Where J_z is the vehicle moment inertia and $\ddot{\psi}$ is the second derivative of yaw angle w.r.t time.
For longitudinal forces, it is assumed that the vehicle has rear traction and uses the traction/braking torque T_d as input. If $T_d > 0$, traction is generated; otherwise, braking is generated.

$$F_x = \frac{T_d}{r_w} \tag{2.10}$$

r_w is the wheel radius.
In addition, longitudinal resistance should be taken into account. Roll resistance is just considered in this case.

$$F_r = R_r V_x \tag{2.11}$$

Where R_r is the total rolling resistance. Due to simplification, longitudinal and lateral aerodynamic drags are removed.
Considering the forces acting on the vehicle as well as some kinematic relations in the vehicle, we can summarize the following relationships, which include six states for the vehicle considering both lateral and longitudinal dynamics. In these equations, t is a continuous time variable.

$$\dot{X}(t) = V_x(t)\cos(\psi(t)) - V_y(t)\sin(\psi(t)) \tag{2.12a}$$
$$\dot{Y}(t) = V_x \sin(\psi(t)) + V_y(t)\cos(\psi(t)) \tag{2.12b}$$
$$\dot{V_x}(t) = \frac{F_x(t) - F_y^f(t)\sin\delta(t) - F_r(t)}{m} \tag{2.12c}$$
$$\dot{\beta(t)} = \frac{F_y^f \cos(\delta(t)) + F_y^r(t)}{mV_x(t)} - r(t) \tag{2.12d}$$
$$\dot{\psi} = r(t) \tag{2.12e}$$
$$\dot{r}(t) = \frac{aF_y^f(t)\cos(\delta(t)) - bF_y^f(t)}{J_z} \tag{2.12f}$$

In the equation (2.12), several simplified assumptions have been taken into account.
Throughout this thesis, a vehicle model of this type is used. As a result, the model was rewritten to include states, inputs, outputs, and model parameters. Noises are ignored.

$$z(t) = \begin{bmatrix} X(t) \\ Y(t) \\ V_x(t) \\ \beta(t) \\ \psi(t) \\ r(t) \end{bmatrix} \quad ; U(t) = \begin{bmatrix} T_d(t) \\ \delta(t) \end{bmatrix} \quad ; \theta = \begin{bmatrix} m \\ J_z \\ a \\ b \\ C_f \\ C_r \\ r_w \\ \mu \\ R_r \end{bmatrix} \tag{2.13}$$

Where $z(t)$ are the states of the model, $U(t)$ is the input, and θ are the model parameters.

Hence, the compact vehicle model can be written as follows:

$$\dot{z}(t) = f_z^{CT}(z(t).u(t), \theta) \tag{2.14}$$

In addition, torque and steering angle as inputs are saturated due to the vehicle's physical limits.

$$\begin{aligned} |\delta(t)| &\leq \overline{\delta} \\ T_{d,min} \leq T_d(t) &\leq T_{d,max} \end{aligned} \tag{2.15}$$

This vehicle model is continuous, and nonlinear. In addition, the value of model parameters can be found in table (A.1).
This model is implemented in MATLAB and Simulink.

2.1.2. Linear Bicycle Model

The linear model illustrates the motion of vehicle under the following conditions: low lateral acceleration, and rigid suspension [24].
As illustrated in non-linear model of vehicle (2.1.1), following are the equations describing force and moment balance:

$$m(\dot{V}_y + V_x.r) = F_y^f \cos\delta + F_y^r \tag{2.16}$$

$$J_z\dot{r} = aF_y^f \cos(\delta) - bF_y^r \tag{2.17}$$

Assuming, small steering angles, $cos\delta$ can be linearized around $\delta = 0$. Therefore, the force and moment balance equations become:

$$m(\dot{V}_y + V_x.r) = F_y^f + F_y^r \tag{2.18}$$

$$J_z\dot{r} = aF_y^f - bF_y^r \tag{2.19}$$

In addition, A linear relationship is assumed between the lateral force generated by the tires and the slip angle.

$$F_y^f = -C_f\alpha_f \tag{2.20}$$

$$F_y^r = -C_r\alpha_r \tag{2.21}$$

Linear stiffness can only be assumed for small slip angles. Accordingly, this assumption is valid only for maneuvers with low lateral accelerations.

The equations (2.4), (2.3), and (2.1) can be linearized. As for small angles $tan(x) = x$. Therefore,

$$w_f = \frac{V_y + ar}{V_x} - \delta \tag{2.22}$$

$$w_r = \frac{V_y - br}{V_x} \tag{2.23}$$

$$\beta = \frac{V_y}{V_x} \tag{2.24}$$

It should be taken into consideration that at $V_x = 0$ the singularity occurs. Due to this, the model is only valid for non-zero longitudinal speeds.
By using lateral velocity and yaw rate as state variables, we can develop linear differential equations.

$$\dot{V_y} = \frac{(-C_f - C_r)V_y + (-C_f a + C_r b - mV_x^2)r}{mV_x} + \frac{C_f \delta}{m} \tag{2.25}$$

$$\dot{r} = \frac{(-C_f a + C_r b)V_y - (C_f a^2 + C_r b^2)r}{J_z V_x} + \frac{C_f a \delta}{J_z} \tag{2.26}$$

State-space form:

$$\begin{bmatrix} \dot{V_y} \\ \dot{r} \end{bmatrix} = \begin{bmatrix} \frac{-C_f - C_r}{mV_x} & \frac{-C_f a + C_r b}{mV_x} - V_x \\ \frac{-C_f a + C_r b}{J_z V_x} & \frac{-C_f a^2 - C_r b^2}{J_z V_x} \end{bmatrix} \begin{bmatrix} V_y \\ r \end{bmatrix} + \begin{bmatrix} \frac{C_f}{m} \\ \frac{C_f a}{J_z} \end{bmatrix} \delta \tag{2.27}$$

This is the final state-space form of the vehicle, whose states are lateral velocity and yaw rate and the input is steering angle. This model is used to design the yaw rate controller which will be explained in section (3.1.2).

2.2. Reference Path Model

One of the challenges for autonomous vehicles is finding an appropriate path to reach their goal position without colliding. There are two types of searching: geometric methods and graph search methods. Path planning, however, is not the focus of this thesis, since paths are predefined and input to path-following algorithms. Therefore, given the path, some characteristics should be exploited. We take into account three characteristics of the path: the curvature, the tangential angle, and the total distance passed on the path.
Reference paths are the crucial link between the planning system and the lateral control system. There are multiple ways to define it.

- It is easiest to define a sequence of straight-line segments using linear connections between points. It is very easy and compact to construct such a path definition.

Despite this, the path contains discontinuities in heading that make precise tracking difficult.

- Waypoints are another option. Discretizing is usually determined by distance or travel time. It is possible to restrict the relative position of the waypoints in order to satisfy an approximate curvature constraint.
- Continually parameterized curves can also be used to define a path. These curves provide the benefit of continuously varying and smooth motion. As a result, the errors are more consistent.

In this study, GPS data of real paths are used. As a result, waypoints are the best option for defining the path. $P_i = [x_i, y_i]$ is the vector of the points forming the path. As a consequence, moving along the vector means moving along the path [1].
The circle passing through all three corners of the triangle formed by the neighboring points P_i, P_{i-1}, P_{i+1} is called the circumscribed circle of the triangle.

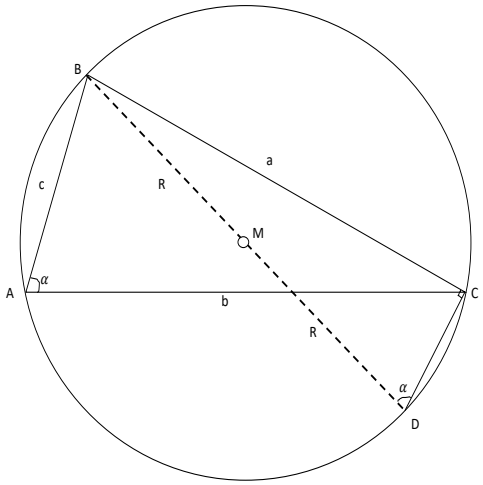

Figure 2.2: Circumscribed Circle

In a Cartesian coordinate system, A, B, and C correspond to the neighboring points in a vector points of path. The length of the side opposite point A is denoted as a, similarly, b and c. α is the angle between AB and AC.
According to figure (2.2), the triangle lies within the plane defined by these three points. A circumscribed circle's center M is equally distant from all corners, thus located at the midpoint between AC and AB normals.
The cross product:

$$D = (B - A) \times (C - A) \tag{2.28}$$

is normal to the triangle plane, pointing toward viewer. The norm of D is :

$$\|D\| = bc \sin(\alpha) \tag{2.29}$$

The line BD runs through the center of the circumscribed circle (M). Angles BAC and BDC are equal, since they are inscribed angles covering the same arc BC.

$$\frac{a}{2R} = \sin(\alpha) \tag{2.30}$$

The area of ABC is:

$$(ABC)_{area} = \frac{1}{2}bc\sin(\alpha) = \frac{abc}{4R} \tag{2.31}$$

Therefore:

$$R = \frac{abc}{4(ABC)_{area}} = \frac{abc}{2\|D\|} \tag{2.32}$$

Finally, the curvature at point P_i is defined as:

$$\kappa_i = \frac{1}{R_i} \tag{2.33}$$

Then, the vector of curvatures $K = [\kappa_i]$ is formed for each position on the path. For infinite values of R, the curvature is considered zero.
The following equation (2.34) can be used to calculate the tangent angle of the path at each point, which is the angle between the line connecting the point to its predecessor and the global X-axis.

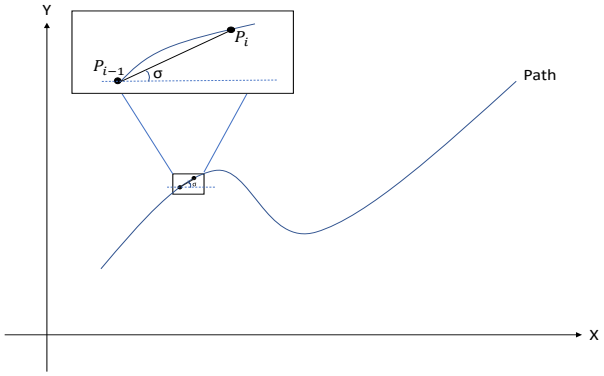

Figure 2.3: tangent angle of path

considering two points $P_i = [x_i, y_i]$ and $P_{i-1} = [x_{i-1}, y_{i-1}]$:

$$\sigma_i = \arctan\left(\frac{y_i - y_{i-1}}{x_i - x_{i-1}}\right) \tag{2.34}$$

$S = [\sigma_i]$ is the vector of the tangent angle of the path at each position P_i which will be used in lateral controller for path following.
Lastly, the distance traveled along the path is calculated at each point along the path. This distance is from the starting point to the target position. Thus, the distance travelled up to P_i is as follows:

$$l_i = l_{i-1} + \|P_i - P_{i-1}\| \tag{2.35}$$

Where l_{i-1} is the distance passed up to P_{i-1}. Then, vector $L = [l_i]$ is the vector of distances at each point.
Finally, these three properties of path (K, S, L) are inputs to the path following algorithm. These characteristics are used for both lateral and longitudinal control of a vehicle. Having said that, these are three vectors that are of the same size. This equals the number of way points on the path since each point on the path has its own curvature, tangent angle and travelled distance.
Taking into consideration that there shouldn't be a small number of waypoints on the path, as this may cause the controller to malfunction. In contrast, a large number waypionts increases computational complexity and slows down path following algorithm. Due to this, the distance between discrete points can be chosen according to the path. In this study, however, the distance between discrete waypoints is kept constant to ensure consistency during different tests.
To extract data from real paths, OpenStreetMap is used. The paths are selected in OpenStreetMap and then imported into MATLAB's drivingScenarioDesigner App. As a result, the center line of each path is extracted and converted to a geometrical curve, while transferring the Cartesian coordinate. Then, as described in this section, the properties of path are calculated as inputs to path following algorithm. (see figure 2.4)

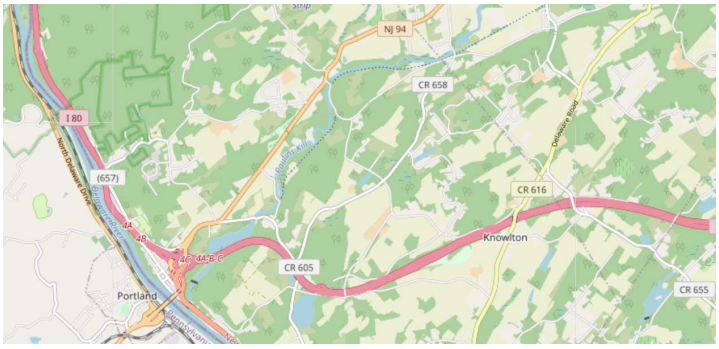

(a) Road on OpenStreetMap.

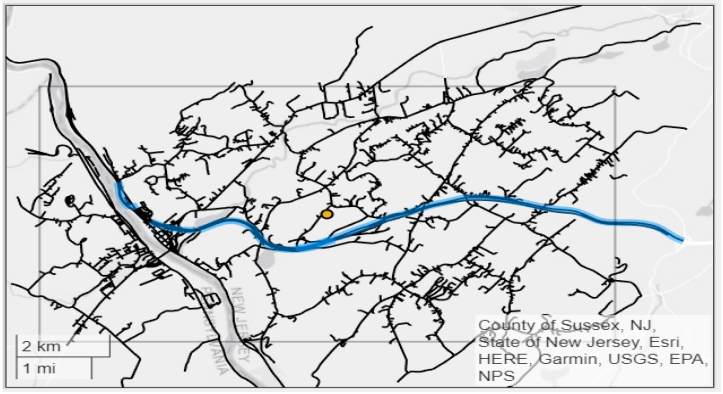

(b) Import road in drivingScenarioDesigner app in MATLAB (blue line) .

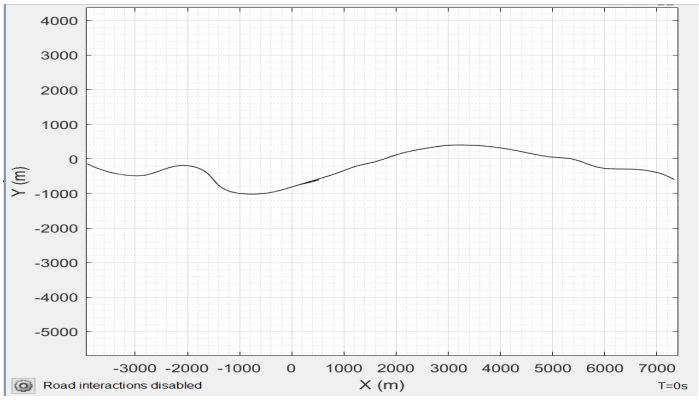

(c) Center line of the road .

Figure 2.4: Extraction of roads from OpenStreetMap

3 | Control Design

Vehicle motion control problems can be divided into three categories. These are the vehicle stabilization of fixed positions, trajectory planning, and the path following problem. When aiming to automatically drive a vehicle, it is possible to formulate the problem as either a trajectory tracking problem or a path following problem [30].

Trajectory planning is a function of time. This means that every point on the path takes place at a specific point in time, whereas path-following is concerned with keeping the vehicle on the predefined path for as long as possible. As well as following a path, autonomous vehicles must stabilize their dynamics. Hence, the path-following controller should be integrated with vehicle dynamics in this study. The closed loop driver model describes this interaction.

A human driver collects information about the vehicle's speed, direction, and position as well as the road, and then adjusts the steering wheel angle and torque/brake values accordingly, to keep the vehicle moving in the same direction of road.

On straight lanes, the driver tries to accelerate the vehicle's speed. Prior to entering a corner, vehicles move at the maximum speed. Before reaching the corner, the driver reduces speed in order to ensure passengers' safety and comfort. This is accomplished by a longitudinal speed controller. It uses the kinematic relations of the vehicle to adjust the speed based on the corners of the road. It will elaborated in section (3.2.1).

Moreover, the driver changes the steering wheel of the vehicle to match the heading angle of the road and vehicle. As a result, the vehicle does not deviate much from the center line. In some studies, the vehicle's heading angle is compared to the current path's heading angle. The model does not provide an accurate representation of the driver. It is more realistic to preview the path and then compare the heading angles at a preview distance. It will be discussed in section (3.1).

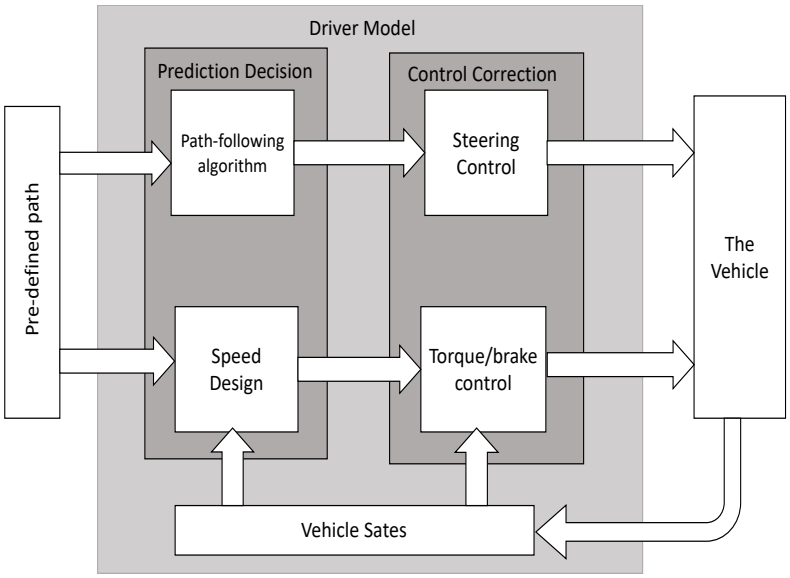

Figure 3.1: Driver model structure

3.1. Lateral Control

A major goal of lateral control is to ensure that the vehicle follows a predefined path. As a result, it should adjust the steering angle in order to correct any errors that occur between vehicle and path. This requires us to determine the error between the vehicle and the predefined path. Next, select a control strategy that reduces the error to zero while taking into account the vehicle's dynamic limitations, such as maximum lateral acceleration and minimum jerk.

When there is more than one measurement, but only one control variable, cascade control is used. The cascade controller consists of two loops: an inner loop and an outer loop. In general, cascade control is used to make sure that disturbances are quickly rejected before they propagate into other parts of the plant and may cause problems. Cascade control is used for lateral control in this study since we have two measurements, yaw and yaw rate, and one input, steering angle. In the inner loop, the purpose is to control the yaw rate, while in the outer loop, the purpose is to ensure that the desired yaw rate is generated as a setpoint for the inner loop. The vehicle position error and heading error are inputs to the outer control.

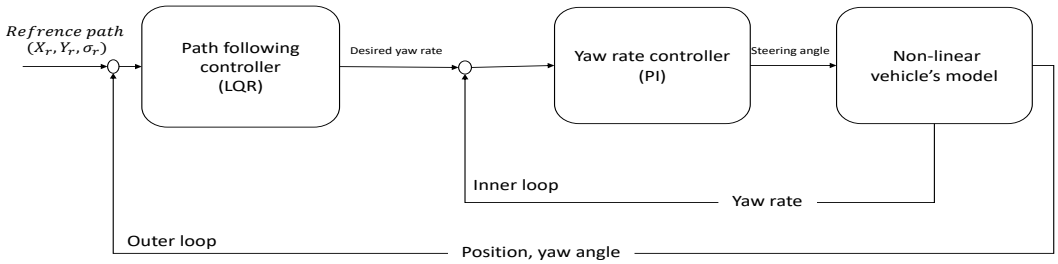

Figure 3.2: Lateral Control structure

3.1.1. Path-following Controller

This is the outer loop of the lateral control. Linear Quadratic Regulator (LQR) approach is used to design the output of the controller, which is the desired yaw rate.

Path-following Model

To design the path following controller, the first thing that needs to be determined is the kinematic relation between the path and the vehicle [19]. The process will be carried out in Serret-Frenet frame. $\Delta\psi$ Is the heading error, which is determined by the difference between the heading angle of the vehicle when viewed from a look-ahead distance and the tangent angle of the path when viewed from a look-ahead distance. e_y is the lateral position error which is the lateral difference between the position of the vehicle and the path at look ahead distance. (see figure 3.3)

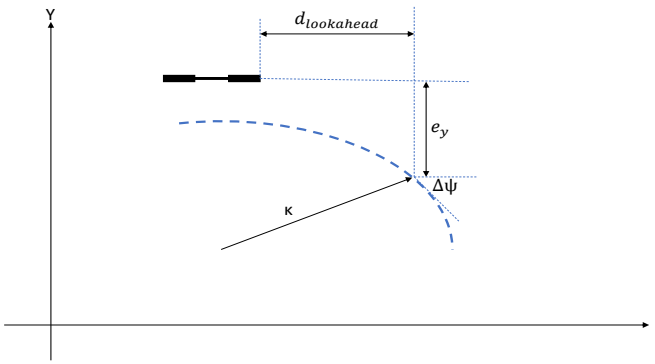

Figure 3.3: Path-following model

It is very important to choose the right look-ahead distance. When the look-ahead point is too far in front of the vehicle, it will be unsuitable to act on the preview information immediately, and the preview information has already been lost by the time it needs to be used. The reverse is also true, if the look-ahead point is too close to the vehicle, then the vehicle will have very poor control, especially when the vehicle is traveling at a high speed. Look-ahead distance can be calculated as follows:

$$d_{lookahead} = T_{driver} V_x \tag{3.1}$$

Where V_x is the longitudinal velocity of vehicle and T_{driver} is the reaction time of driver which is different in every driver. Here, it is considered as $0.3\,s$. This means that the look-ahead distance depends on the vehicle's speed. The higher the speed of the vehicle, the longer the preview distance is needed because the driver has to react faster if an obstacle comes into view in case of an emergency. In contrast, when the velocity is low, the shorter look-ahead distance is sufficient.

The use of a single preview point for describing a driver model is considered impractical by many researchers [15]. Even with a proper look-ahead distance, a single preview-point model can generate data that is not consistent with the vehicle's present state, especially if the road profile is complicated. (see figure 3.4). Moreover, in reality, a driver does not get all the information based on one point in front of him. Instead, the driver controls the vehicle using a series of preview points.

In this case, path's reference yaw angle is not based on a single preview point, but on an average of all preview points. A lateral error is also calculated by taking into account the average of the lateral positions of all preview points in order to determine the lateral error (see figure 3.4).

Five preview points are selected between the current position of the vehicle and the look-ahead distance in this thesis. These five points are located on the longitudinal axis of the vehicle. As a result, these preview points can be calculated as follows:

$$X_{pp,i}(t) = x(t) + K_i.d_{lookahead}.\cos\psi(t) \tag{3.2a}$$

$$Y_{pp,i}(t) = y(t) + K_i.d_{lookahead}.\sin\psi(t) \tag{3.2b}$$

Where $x(t)$ and $y(t)$ is the position of vehicle at time t. $X_{pp,i}$ and $Y_{pp,i}$ are the coordinates of i_{th} preview point. K_i is the order of the preview point which is between one to five. $d_{lookahead}$ is defined in (3.1) and $\psi(t)$ is the heading angle of vehicle at time t.

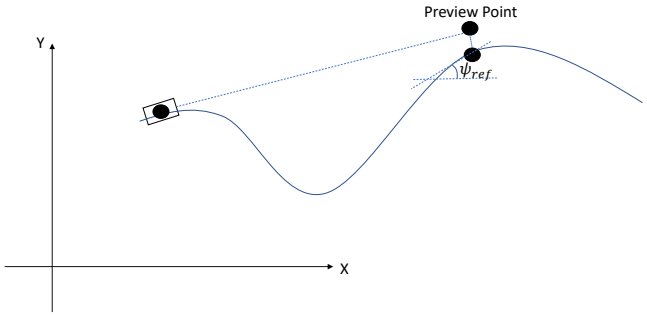

(a) Single Preview Point.

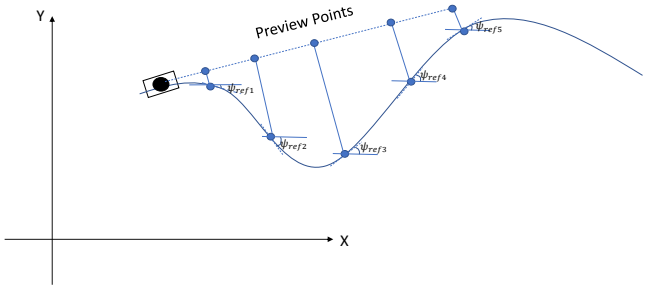

(b) Multi Preview Points.

Figure 3.4: Comparison of single preview-point and multi preview-points [15]

Once this has been done, the relevant point on the desired path should be chosen which corresponds to the preview point. This is the closest point on the path to the preview point.

Next, the lateral position and yaw angle errors should be calculated. Initially, the tangent angles of these five points of the desired path are selected from the vector of reference tangent angles discussed in equation (2.34), and their averages are determined and named $\psi_{ref}(t)$. In addition, the lateral positions of these five points are also averaged and named

$y_{ref}(t)$. Finally, the error is calculated at every time in the following manner:

$$\Delta\psi = \psi_{ref}(t) - \psi(t) \tag{3.3a}$$
$$e_y = y_{ref}(t) - y(t) \tag{3.3b}$$

Where $\psi(t)$ is the heading angle of vehicle at time t and $y(t)$ is the lateral position of vehicle at time t. As a result, these errors are inputs to the path following controller.

Control Design

The path-following model for autonomous vehicles based on the Serret-Frenet framework is [9], [19]:

$$\dot{e_y} = \quad V_x\Delta\psi + d_{lookahead}r + V_y \tag{3.4a}$$
$$\Delta\dot{\psi} = \quad r - V_x\kappa(s) \tag{3.4b}$$

Where V_x is the longitudinal velocity and V_y is the lateral velocity of vehicle. r is the yaw rate and κ is the curvature of the path at related position. $d_{lookahead}$ is defined in (3.1). These equations (3.4) is then transformed into state space form. Where $X = [e_y \quad \Delta\psi]^T$ is the state of the system, $u = r$ yaw rate is the control input and the disturbance is $w = [v_y \quad -v_x\kappa(s)]^T$.

$$\begin{aligned} \dot{X}(t) &= AX(t) + Bu(t) + w \\ y(t) &= CX(t) \end{aligned} \tag{3.5}$$

Then,

$$A = \begin{bmatrix} 0 & V_x \\ 0 & 0 \end{bmatrix}, B = \begin{bmatrix} V_x d_{lookahead} \\ 1 \end{bmatrix}, C = \begin{bmatrix} 1 & 0 \\ 0 & 1 \end{bmatrix}, w = \begin{bmatrix} V_y & -V_x\kappa(s) \end{bmatrix} \tag{3.6}$$

Outputs of the system are lateral position error and heading angle error. Due to lateral velocity and curvature of path being treated as disturbances here, a suitable control design should be provided in order to deal with disturbances and provide accurate path following. In cascade control, the inner loop deals with disturbances, which will be discussed in the next section (3.1.2).
It is possible to define a state feedback controller as:

$$u = -Kx \tag{3.7}$$

Where K is the state feedback gain.
It should be noted that a time varying parameter in the system model is longitudinal velocity, which varies between a minimum and a maximum $[V_{xmin}, V_{xmax}]$. Therefore, V_x

can be written as:

$$Vx = h_1 V_{xmin} + h_2 V_{xmax} \tag{3.8}$$

Where

$$h_1(t) = \frac{V_x(t) - V_{xmin}}{V_{xmax} - V_{xmin}}, \quad h_2(t) = \frac{V_{xmax} - V_x(t)}{V_{xmax} - V_{xmin}}, \quad \sum_{i=1}^{i=2} h_i(t) = 1, \quad h_i(t) \geq 0 \tag{3.9}$$

It is possible to revise the state-space model as follows:

$$\begin{aligned} \dot{X}(t) &= \sum_{i=1}^{i=2} h_i(t)((A + BK)X(t) + w) \\ y(t) &= CX(t) \end{aligned} \tag{3.10}$$

As a result, the state feedback controller will be modified:

$$K = \sum_{i=1}^{i=2} h_i(t) K_i \tag{3.11}$$

K_1 is designed when V_{xmin} is used in the model of the system, and K_2 is designed when V_{xmax} is used in the model of the system.
Then, the desired yaw rate is as following:

$$r_d = \sum_{i=1}^{2} h_i(t) K_i X \tag{3.12}$$

State feedback controller is designed using Linear Quadratic Regulator (LQR). Considering the state-space form of system in equation (3.5) with $x \in \mathbb{R}^n$, $u \in \mathbb{R}^n$, and x_0. Linear quadratic regulators with finite horizons are given by the following equations:

$$J = \int_0^T (x'(\tau)Qx(\tau) + u'(\tau)Ru(\tau)d\tau + x'(T)Sx(T) \tag{3.13}$$

where $Q \geq 0, R > 0, S \geq 0$ are symmetric, positive (semi-) definite matrices. x is the state of the system and u is the system input.
HJB equations can be employed to minimize this cost function [16] which results in the differential Riccati equation.

$$\begin{aligned} &\dot{P}(t) + Q - P(t)BR^{-1}B'P'(t) + P(t)A + A'P'(t) = 0 \\ &P(T) = S \end{aligned} \tag{3.14}$$

Then, finite horizon control law can be defined as:

$$u(t) = -R^{-1}B'P'(t)x(t) = -K(t)x(t) \tag{3.15}$$

It should be noted that $K(t)$,the gain of controller, is time varying over the finite interval which makes solving the differential equation hard and it's not easy to apply it to standard control problems due to the stabilization problems. The idea is to eliminate the terminal constraint and $T = \infty$. Therefore, the problem turns into:

$$\begin{aligned} J &= \int_0^\infty (x'(\tau)Qx(\tau) + u'(\tau)Ru(\tau)d\tau \\ Q &= Q' \geq 0 \quad R = R' \geq 0 \end{aligned} \tag{3.16}$$

Then, if the pair (A, B) is reachable in the system (3.5), the solution of differential Riccati equation for $T \to \infty$, tends to a constant matrix $\bar{P}$. The equation in (3.14) turns into *algebraic Riccati equation* as following :

$$0 = A'\bar{P} + \bar{P}A + Q - \bar{P}BR^{-1}B'\bar{P} \tag{3.17}$$

The asymptotic control law is:

$$u(t) = -R'B'\bar{P}x(t) = -\bar{K}x(t) \tag{3.18}$$

This is a time-invariant control law that simplifies the design process. It does not yet yield stabilization, and weight matrices of states are needed to ensure it.
The weight matrix of states (Q) can be chosen in many ways. If the pair (A, C) in the system (3.5) can be observed, we can define Q as:

$$Q = C'C \tag{3.19}$$

Which guarantees the stability of the system. The proof can be found in [16].
The choice of R should be made in such a way that it fulfills our aim of lateral cascade control which will be discussed in the section (4.3).

3.1.2. Yaw Rate Controller

In this section, the design of the yaw rate controller (inner loop) will be discussed in detail. Inner loop setpoint is yaw rate, which is defined in equation (3.12) and is the output of

Linear Quadratic Regulator (LQR) controller. As a result, the inner loop controls the yaw rate of the vehicle. The steering angle of the vehicle is the output of the controller. Proportional-Integral (PI) controllers are used for this purpose. PI is a feedback controller that maintains a set point regardless of disturbances or changes in the plant. The output is calculated based on the error measurement.
Therefore, proportional control can accelerate settling and integral control can reduce constant error.
PI controller can be defined as:

$$u(t) = K_p e(t) + K_i \int_0^t e(t)dt \tag{3.20}$$

Where $e(t)$ is the yaw rate error and vehicle input is $u(t)$, which is steering angle.
Or as a transfer function in continuous time:

$$K_p + \frac{K_i}{S} \tag{3.21}$$

Where K_p is the proportional gain and K_i is the integral gain.
As the last step in the process, it is important to choose the control parameters that will allow the vehicle to track the path and have a stable dynamic. Three parameters need to be designed. In outer loop, R comes from Linear Quadratic Regulator (LQR) control, whereas in inner loop, Kp and Ki come from Pl controller.

It should be taken into consideration that when designing cascade control, it is necessary to first design the inner loop. Then after determining the parameters of the inner loop, the outer loop can be designed. According to rule of thumb, the inner loop should be at least 3-10 times faster than the outer loop.

It is possible to design a controller based on the frequency response of a system. The frequency response of a system describes how it responds to sinusoidal inputs of varying frequencies and is used to analyze and design control systems. Linear Time-Invariant (LTI) systems produce steady state output when sinusoidal signals are applied as inputs. This steady state output is also a sinusoidal signal. The input and output sinusoidal signals have the same frequency, but different amplitudes and phase angles.

Bode plots are commonly used to determine a control system's stability. Bode plots are used to map the frequency response of the system with the help of two graphs - the Bode magnitude plot and the Bode phase plot (see figure 3.5).

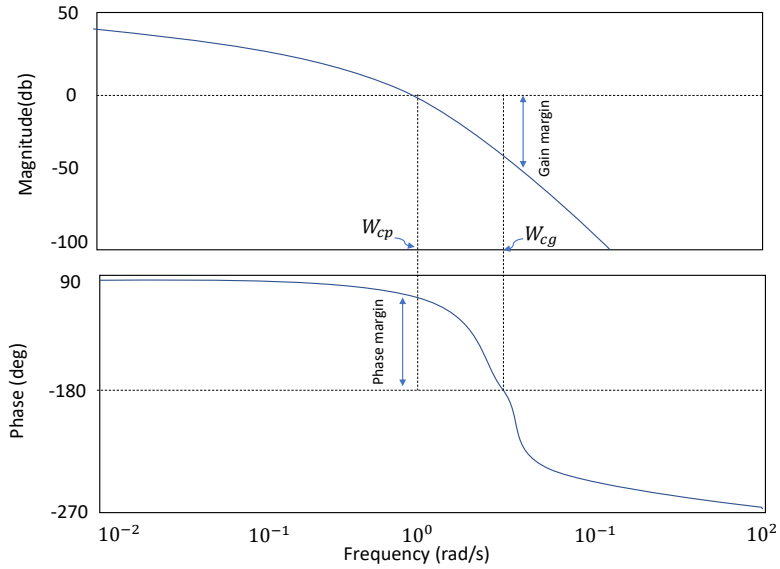

Figure 3.5: Bode diagram

In order to analyze the properties of a feedback control system, two important parameters to consider are the gain margin (g_m) and phase margin (φ_m). Their definition can be seen in figure (3.5). In addition, The gain cross-over frequency W_{cg} is the frequency at which the magnitude of open loop system is unity.
Usually, the regulator must guarantee : [16]

- $\varphi_m \geq \bar{\varphi_m}$
- $g_m \geq \bar{g_m}$
- $W_{cg} \geq \bar{W}_{cg}$ In order to ensure a satisfactory response time, tracking of reference, and attenuation of disturbance.

The margins should be positive in order to have a stable system, but the greater the margins, the more stable the system will be. For a robust controller, phase margin and gain margin should be larger than a certain value ($\bar{\varphi_m}$ and $\bar{g_m}$). It is important to note that the crossover frequency W_{cg} approximates the control bandwidth. Closed-loop response time is proportional to $\frac{1}{W_{cg}}$.

Thus, in this thesis, W_{cg} plays an important role in designing inner loop controller and outer loop controller, as the inner loop should be at least 10 times faster, and hence the cross-over frequency should be at least 10 times higher.

The linear bicycle model of a vehicle in section (2.1.2) is used to design the control parameters of the yaw rate controller. It should be taken into account that the longitudinal

speed of the vehicle is a variable parameter. Therefore, the model of the system is constantly changing. It is decided to take the average speed (around 35 km/h) and use that as a constant value for the system model. Yaw rate controller can handle varying systems because they are designed based on PIDs.

In this case, the gain margin of the vehicle model is infinite without any controller. Infinite gain margin means no matter how much you increase the gain of the controller, the system will be stable anyway. As a result, the inner loop is chosen to be around 100 times faster than the outer loop. It has been observed, however, that faster settling times than this in the inner loop don't affect system performance.

Therefore, the PI controller is designed with a cross-over frequency of 200. As a result:

$$K_p = 3, \quad K_i = 10.5 \tag{3.22}$$

The bode diagram of the open loop system is as following:

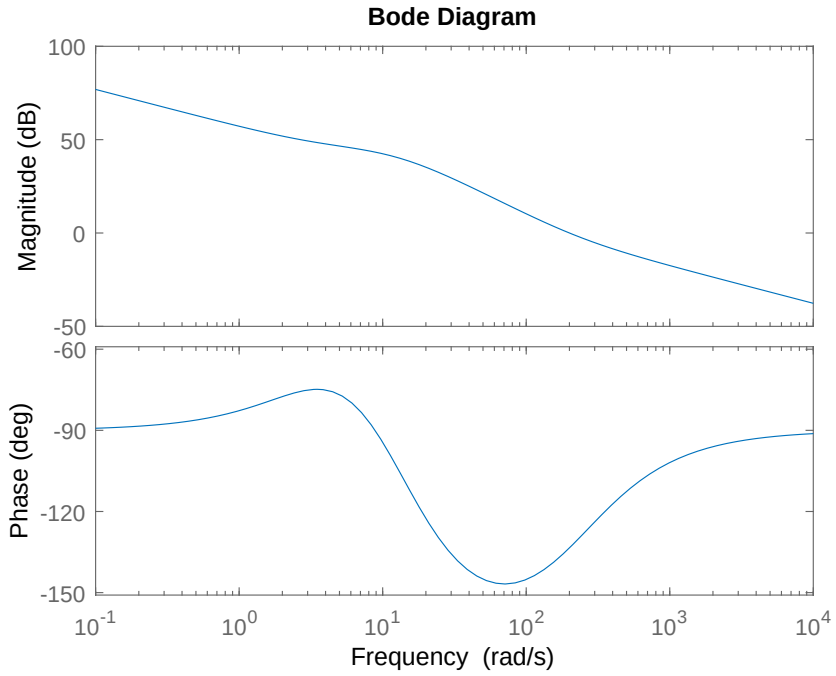

Figure 3.6: Bode diagram of open loop system

Where $\varphi_m = 38.6°$ and $g_m = \infty$.

As previously mentioned, R from Linear Quadratic Regulator (LQR) controller in the

outer loop should also be designed. It is one of the optimization variables that will be discussed in section (4.3). However, the range is concluded here in order to compare the outer loop's response time with the inner loop's. R is chosen from 100 to 200 as the settling time varies between 4.9 seconds and 5.9 seconds.

The inner loop response time is compared to the outer loop response time in the following. The settling time of inner loop is 0.044 seconds and outer loop is 4.89 seconds (with R=100) see figure (3.7).

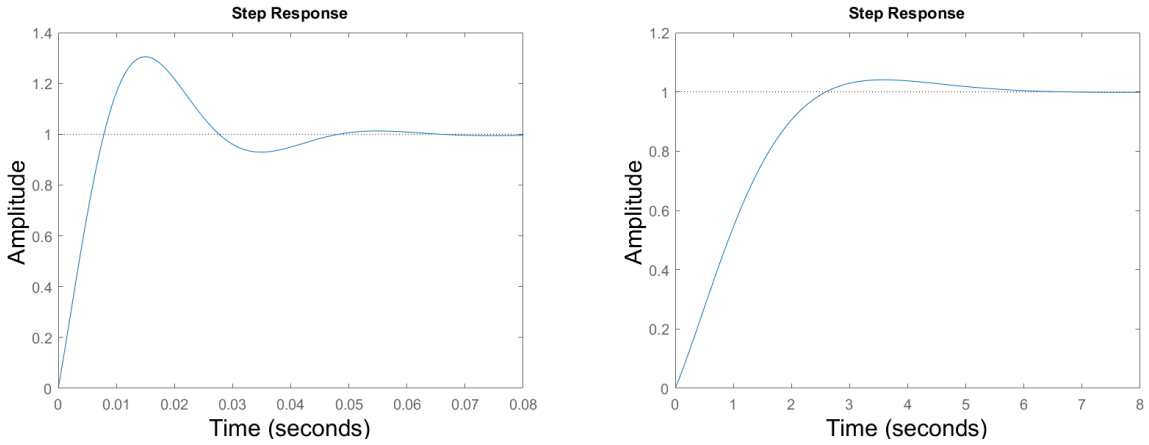

(a) Inner loop step response.

(b) Outer loop step response.

Figure 3.7: Comparison of inner loop step response and outer loop step response of cascade loop in lateral control.

3.2. Longitudinal Control

The longitudinal controller of the vehicle is composed of two parts. A speed profile design is first established and a cruise control system is used to follow the reference speed.

3.2.1. Speed Profile Design

In autonomous driving applications, speed planners play a crucial role. We need to obtain a speed plan that provides high comfort and low travel time while tracking the planned path with minimum error.

The driver should ensure that proper speed is maintained when following the path, especially when entering corners. The longitudinal speed and the lateral acceleration of a

vehicle are related as following:

$$\kappa = \frac{a_y}{V_x^2} \tag{3.23}$$

Therefore, with a known maximum lateral acceleration, the speed based on the curvature of the path at each position P_i can be defined as following:

$$V_{x,curv,i} = \sqrt{\frac{a_{y.max}\mu_y}{|\kappa_i|}} \tag{3.24}$$

Where κ_i is the curvature of the path at position P_i, then $a_{y.max}$ is the maximum lateral acceleration of vehicle, and μ_y is the lateral tyre-road friction. $a_{y.max}$ can be defined in different ways, however it is chosen to be 3.70 m/s^2 in [18] based on Battelle study. μ_y is considered as 0.85 (dry asphalt.)

On the other hand, it should be noted that every road has a maximum speed that is mandatory by law. Thus, the vehicle's reference speed cannot be greater than the law maximum speed. Finally, the reference speed is defined as follows:

$$V_{ref,i} = \max(V_{maximum}, V_{x,curv,i}) \tag{3.25}$$

Therefore, for each point on the reference path, a relevant speed is calculated based on corresponding curvature (κ_i). (see figure 3.8)

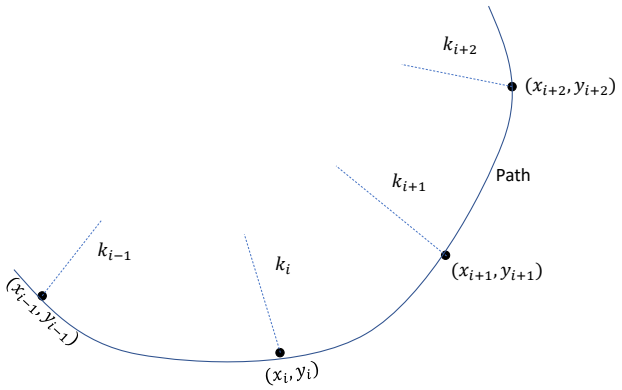

Figure 3.8: Curvatures of path points

In the same way that lateral control is designed using the preview distance in equation

(3.1), the speed is predicted in the look ahead distance. Therefore, the reference speed is the input of longitudinal controller based on the curvature of the path at the look ahead distance.

In this case, we are going to plan the speed in both offline and online manner. Each position on the path has a reference speed defined based on its curvature, which is saved in a vector of speeds. As a result, when the vehicle reaches the position in look ahead distance, the longitudinal controller employs the relevant reference speed. (see figure 3.9)

In the figure (3.9), speed planner is defined in equation (3.25). In reference speed generator, The preview points on the path are calculated the same way as the equation (3.2). However, only one preview point is chosen. This is the last preview point on the look ahead distance, and the closest point on the path to this preview point is found. Therefore, the output of the reference speed generator is the reference speed of this point on the path determined by the speed planner.

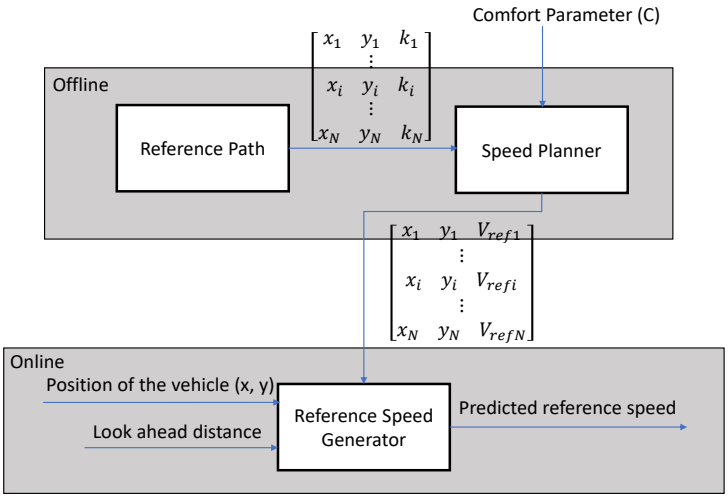

Figure 3.9: Reference Speed diagram [22]

One of the inputs to the speed planner is a comfort parameter. The maximum lateral acceleration is used in equation (3.24). However, the speed calculated from this equation does not guarantee the comfort of passengers. The parameter C is therefore added to the equation to regulate speed and, consequently, passenger comfort. As a result, the equation is modified as follows:

$$V_{x,curv,i} = \sqrt{\frac{a_{y.max}\mu_y}{|\kappa_i|C}} \tag{3.26}$$

Using the proper value of C will reduce the reference speed and provide passengers with more comfort. C is one of optimization variables which will be discussed in section (4.3) For example, with C=5 the speed profile of the path can be seen in figure (3.10).

However, a large C does not necessarily mean the drive will be more comfortable. The high values of C cause rapid speed changes, resulting in high acceleration. Nevertheless, C should remain in the range that will be discussed in section (4.2.4).

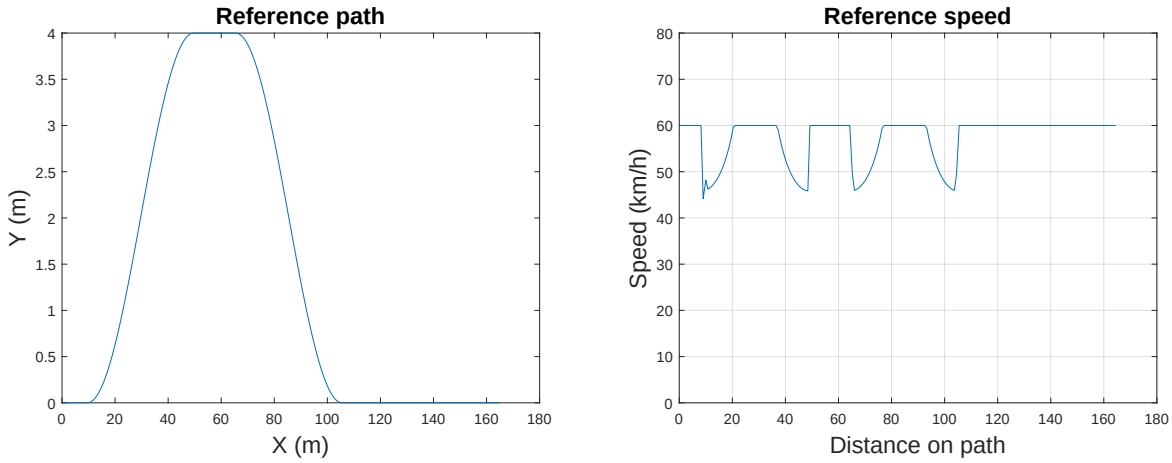

(a) Reference path.

(b) Speed Profile .

Figure 3.10: Speed profile of the path. The total distance is 164.5 m for double lane reference path

Smooth Speed Design

This thesis aims to provide comfortable driving for passengers. One way to achieve this goal is to provide passengers with a smooth speed profile. As a result, passengers do not experience a large reduction or increase in speed during driving. It will be elaborated in section (4.1).

Using the speed planner discussed in this study along with comfort parameter will provide the proper speed for passengers. However, it does not affect the acceleration or deacceleration of the vehicle (acceleration and deceleration effects on comfort are discussed in section (4.1)). Because of this, passengers are not provided with a smooth speed profile.

Next, we will smooth out the speed profile. To achieve this aim, a low pass filter is added to the speed profile after the speed planner. Low pass filters come in many different designs, including Butterworth, Elliptical, Chebyshev, Bessel. The Butterwoth low pass filter is used in this study.

Butterworth filters are designed to have as flat a frequency response as possible in the passband, from $0Hz$ to cut-off frequency ($-3\,dB frequency$). The frequency response will roll-off towards zero if frequency exceeds the cut-off frequency. Butterworth filter's general form is:

$$H(jw) = \frac{1}{\sqrt{1+\epsilon^2(\frac{w}{w_c})^{2n}}} \tag{3.27}$$

Where, w is the passband frequency of the system. w_c is the cut-off frequency. ϵ is the maximum passband gain and n is the order of the filter. ϵ can be defined by following equation:

$$H_1 = \frac{H_0}{\sqrt{1+\epsilon^2}} \tag{3.28}$$

Where H_0 is the maximum passband gain and H_1 is the minimum passband gain. If H_0 defines at a cut-off frequency ϵ equals to one.

It is possible for Butterworth filters to have different orders, resulting in different frequency responses. It should be noted that as the Butterworth filter order increases, the response gets closer to brick walls.

The Butterworth filter transfer function can be normalized at frequency $w_c = 1\,rad/s$. Thus, the normalized Butterworth filter has a general form. Butterworth calculated coefficients of normalized transfer functions with a $1\,rad/s$ cut-off frequency. (table can be found in A.2). With the help of this table, Butterworth transfer functions can be designed for different orders.

First, the Butterworth filter is designed with a passband frequency equal to the sampling frequency. In this case, the value of half of the number of samples is used as the sampling frequency. The number of samples equals the number of waypoints on the path. Next, the cut-off frequency f_c is one of the optimization variables in section 4.2.4. Different cut-off frequencies result in different speed profiles. Here, the order of filter is chosen as 2.

It can be seen that how f_c affect the speed profile. In the figure (3.11) you can see two different speed profiles one for $f_c = 4$ and the other for $f_c = 12$.

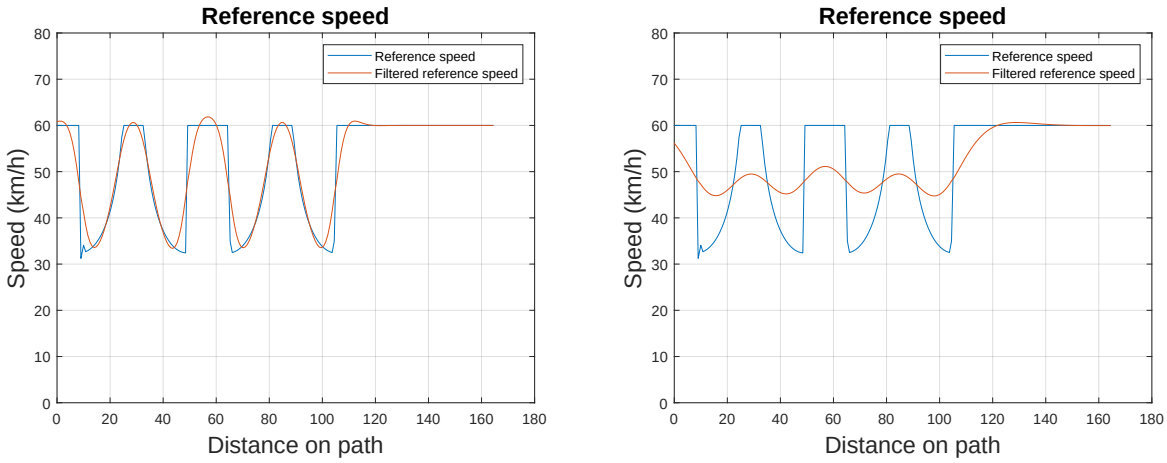

(a) $f_c = 12$ (b) $f_c = 4$.

Figure 3.11: Comparison of speed profiles with different cut-off frequencies

Without filtering, the reference speed has large fluctuations and sharp profile in some parts, which makes the derivative of speed , acceleration, large and then uncomfortable driving. In contrast, it is observed that the filtered reference speed is much smoother, providing a more comfortable driving experience.
It should be noted that due to the C parameter, the reference speeds are much lower than the allowed speed. Therefore, if the smooth speed after filtering is higher than the unfiltered speed, a problem will not occur.

3.2.2. Cruise Control

The cruise control system is one of the most well-known and widely used control applications in autonomous vehicles. Basically, the cruise control system is designed to maintain a fixed reference speed by using torque commands, as well as accelerating or decelerating to a new reference speed. There are now many systems with enhanced features, such as adaptive cruise control, which can adjust the reference point based on measurements taken from a leading vehicle. As an example, traffic assist adjusts vehicle speed to maintain space between vehicles.

Here, the cruise controller is designed to follow the reference speed set by the speed planner. As an input, the controller receives the difference between the actual speed of the vehicle and the reference speed from the speed planner. As an output, it produces the torque that should be applied to the vehicle. Cruise control is designed based on Proportional-Integral (PI) controllers.

First, the longitudinal dynamic of the system (2.12c) is linearized around $40\,km/h$ in order to design the Proportional-Integral (PI) controller. Here is the step response of the linearized system.

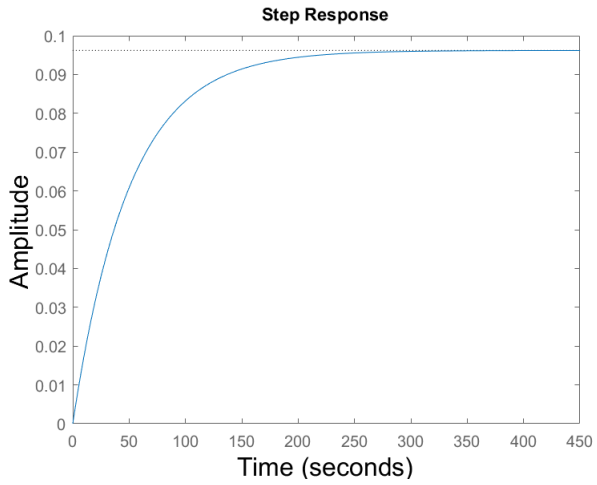

Figure 3.12: Step response of open loop longitudinal vehicle system

It is evident from figure (3.12) that the open loop system is stable, but there is a huge steady state error. Bode diagrams can also be used to calculate steady state error. The DC gain of this system is $-20.33\,dB$ or 0.096.

Steady state error is influenced by the DC gain of a system. Therefore, if we want our steady state error to be less than 1% of reference, the system's DC gain needs to be higher than 99 or $39.9\,dB$. For this reason, the proportional controller should increase the DC gain above $39.9\,dB$ in order to reach the desired steady state error. Therefore:

$$K_p \geq 39.9\,dB + 20.33\,dB = 60.23\,dB \quad or \quad 1026.8 \tag{3.29}$$

Then $K_p = 1030$ is chosen. Applying K_p to the system, the Bode diagram of the open loop is as follows (see figure 3.13):

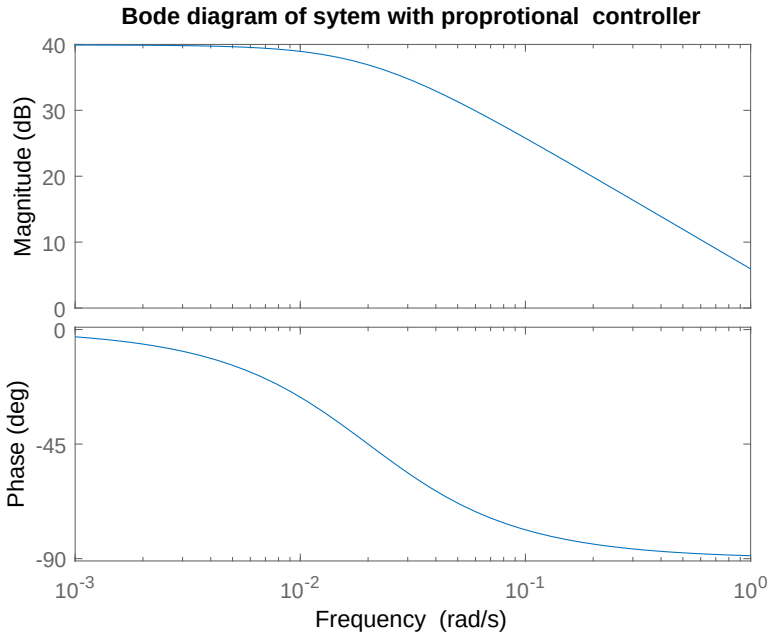

Figure 3.13: Bode diagram of cruise control with proportional gain

As is evident from the figure (3.13) , the DC gain of the system is 39.9 dB.
In addition, the step response of the closed loop system with proportional gain is as follows:

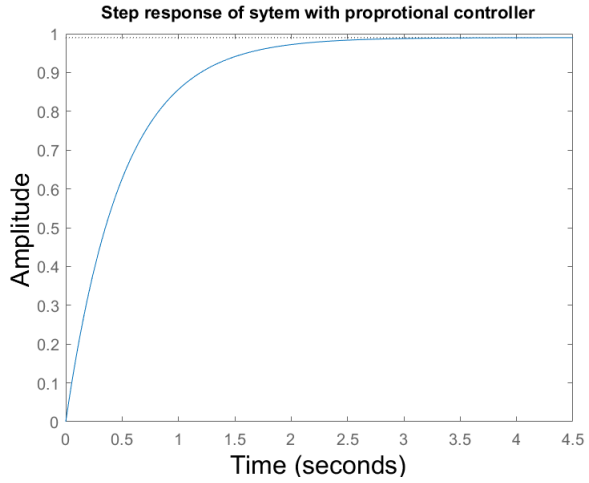

Figure 3.14: Step response of cruise control with proportional gain

In figure (3.14), While the steady-state error is satisfactory, the rise time is too short for

real-world vehicles. Hence, we increase the rise time by using the smaller proportional gain while reducing the steady state error by adding an integral action to the controller.

Then the parameters of the PI controller are selected as follows:

$$K_p = 520 \quad K_i = 9 \tag{3.30}$$

The step response of the system is as follows when using PI controller with these designed parameters:

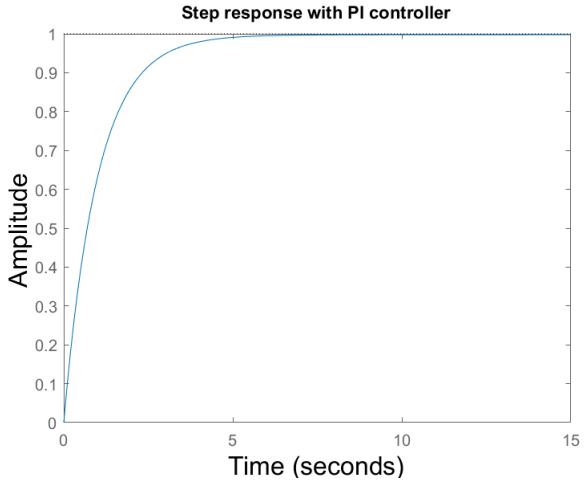

Figure 3.15: Step response of cruise control with PI controller

We can see in figure (3.15) that the steady-state error decreases to zero while the rising time is longer than previously. This is more applicable to real-world vehicles. In addition, an anti-wind up scheme has been added to integral action to prevent saturation in actuators.

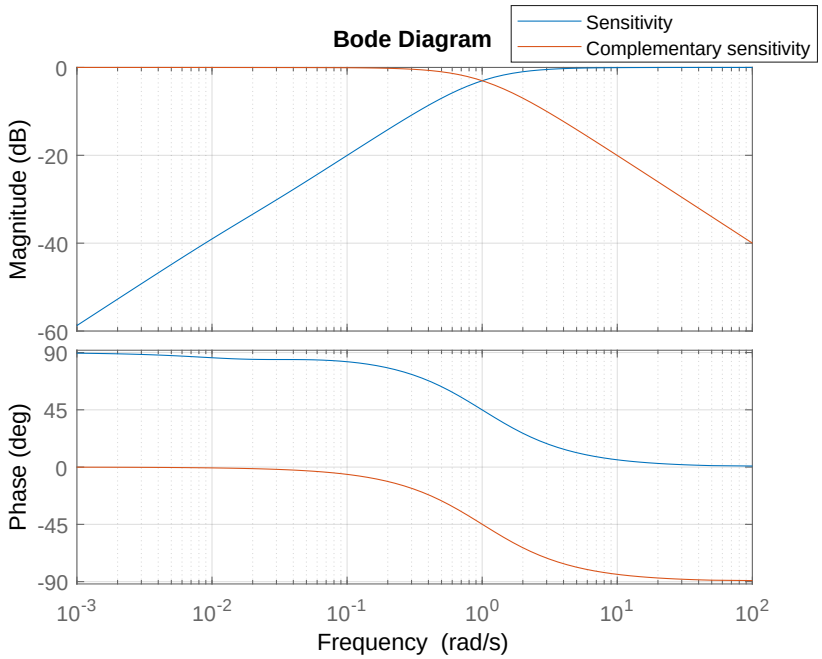

Figure 3.16: Sensitivity and complementary sensitivity functions of the final PI controller with longitudinal dynamic.

4 | Multi-Objective Optimization

This study aims to design a trajectory planning and path-following that follows the path with the smallest possible error while prioritizing passenger comfort and travel time. In order to achieve the goal mentioned above, an optimization algorithm should be applied to the closed loop control system of a vehicle. The closed loop system of a vehicle, however, is highly nonlinear. In this chapter, we discuss first the optimization problem, its cost functions, and constraints, and then a multi-objective optimization is carried out on the closed loop model. Since comfort is the primary objective of this study, it is defined in this chapter first.

4.1. Comfort Definition

Various definitions of comfort are discussed from different studies in section (1.2). However, the comfort definition employed in this thesis is presented here. In the optimization problem, comfort is included both in the cost function and in the constraints. One of the goals of this research is to maximize comfort for passengers. As a result, the comfort objective we are defining is one of the objective functions in multi-objective optimization. The smoother the speed profile of the vehicle, the more comfort is provided for passengers. In [33] Different objectives are tested to see which one provides a smoother speed profile. The third-order temporal derivative of the position is called jerk. There are also fourth-order, fifth-order, and sixth-order derivatives of x(t), but they have little effect on the speed profile. In addition, Speed profile design was carried out with different performance indexes like minimum norm of jerk or minimum square of jerk. As a final result, the metric based on the square of jerk minimization results in a smoother speed profile that means more passengers' comfort, while others have nearly the same results. The smoothness of speed without any sharp change implies that acceleration is continuous and differentiable. Therefore, one of the indexes considered for comfort optimization is the square of longitudinal and lateral jerks.

$$J_{comfort} = \int_0^{T_f} j_x^2 + j_y^2 dt \tag{4.1}$$

while T_f is the total traveled time. However, the indexes are considered in discrete time.

$$J_{comfort} = \sum_{i=1}^{N} j_x(i)^2 + j_y(i)^2 \tag{4.2}$$

where N is the number of samples (waypoints).
In addition, As indicated in section (1.2), motion sickness dose value (MSDV) is another index that measures passengers' comfort. In this case, MSDV is defined based on lateral and longitudinal accelerations. According to ISO 2631-1:1997 [14], the R.M.S acceleration values are defined to reflect the discomfort that humans face. R.M.S acceleration along longitudinal and lateral axes is defined as:

$$a_{RMS} = \sqrt{(k_x w_k a_x)^2 + (k_y w_k a_y)^2} \tag{4.3}$$

$$a_{xRMS} = \sqrt{(k_x w_k a_x)^2} \tag{4.4}$$

$$a_{yRMS} = \sqrt{(k_y w_k a_y)^2} \tag{4.5}$$

The coefficients $w_k = 0.426$ and $w_d = 0.067$ are provided in ISO 2631-1:1997 [14].To evaluate health effects, $k_x = 1.4$, $k_y = 1.4$ are taken from the study [3].
Therefore motion sickness dose value (MSDV) can be defined as:

$$MSDV = \sqrt{\int_0^T a_{RMS}^2(t)dt} \quad m/s^{3/2} \tag{4.6}$$

Then, the illness rate can be defined based on MSDV.

$$IR = \frac{1}{50} * MSDV \tag{4.7}$$

The illness rating (IR) can ranked from zero to three based on how passengers feel. [13]

$IR = 0$	I felt good
$IR = 1$	I felt slightly unwell
$IR = 2$	I felt very bad
$IR \geq 3$	I felt absolutely terrible

Table 4.1: Different comfort levels based on illness rating

Therefore, it can be concluded that smaller longitudinal and lateral acceleration results in a smaller R.M.S value and a lower illness rating. To provide comfort for passengers, the square of lateral and longitudinal acceleration should be minimized. Thus, it will be added to the comfort objective as defined in equation (4.2). The final comfort objective is :

$$J_{comfort} = \sum_{i=1}^{N} j_x(i)^2 + j_y(i)^2 + a_x(i)^2 + a_y(i)^2 \tag{4.8}$$

Additionally, both jerks and accelerations should be limited to ensure the comfort of passengers. In [31] and [26] the limits are provided as follow:

Comfort level	**Acceleration** (m/s^2)	**Jerk**(m/s^3)
comfortable	-2<a<2	-0.9<j<0.9
uncomfortable	-4<a<-2 or 2<a<4	-2<j<-0.9 or 0.9<j<2
dangerous situation	a<-4 or a>4	j<-2 or j>2

Table 4.2: Acceleration and jerk limits

These limits are taken into consideration in the constraints of optimization problem.

4.2. Optimization Problem

As the controllers for the vehicle are designed, the goal is to optimize some control parameters in the closed loop model of the vehicle in order to achieve high comfort and less travel time while path following. This section defines the cost function, constraint and optimization variables of the problem. Afterwards, an algorithm is presented to solve the problem.

4.2.1. Cost Function

As discussed previously, the objective of this optimization is to maximize the comfort of passengers while minimizing vehicle travel time and lateral error of vehicle position from pre-defined path. There is a need for a multi-objective problem due to the conflicting cost functions. Thus, the objective function can be defined as follows:

$$J = w_1 J_1 + w_2 J_2 + w_3 J_3 \tag{4.9}$$

as J_1, J_2, J_3 are the cost functions which will be discussed in the following and w_1, w_2, w_3 are the tuning weights. When different weights are used, each term is prioritized differently, resulting in different outcomes.

Our first cost function will be the vehicle's lateral error relative to the path. A lower lateral error results in more accurate path following. In this way, vehicle will be kept as close as possible to the center line of the road.

$$\begin{aligned} e_y(t) &= y_{ref}(t) - y(t) \\ J_{lateral} &= \sum_{i=1}^{N} e_y(i)^2 \end{aligned} \tag{4.10}$$

Where e_y is the same one that is defined in equation (3.3b) and N is the number of waypoints on the pre-defined path.

The other term refers to minimizing travel time. Aiming to maximize speed as much as possible will minimize travel time. Therefore, J_{speed} will be defined as:

$$J_{speed} = -\sum_{i=1}^{N} V_x(i)^2 \tag{4.11}$$

Where V_x is the longitudinal velocity of vehicle.

Lastly, comfort is a cost function that is discussed extensively in section (4.1).

$$J_{comfort} = \sum_{i=1}^{N} j_x(i)^2 + j_y(i)^2 + a_x(i)^2 + a_y(i)^2 \tag{4.12}$$

4.2.2. Constraints and Optimization Variables

In the optimization problem, a nonlinear bicycle model of the vehicle is used. The inputs of the vehicle are steering angle δ and torque T_d. Therefore, there are saturation constraints on the inputs. The physical capabilities of the vehicle are largely responsible for these limitations.

$$\begin{aligned} \underline{\delta} \leq \delta(i) \leq \bar{\delta} \qquad & for \qquad i = 1, .., N \\ \underline{T} \leq T(i) \leq \bar{T} \qquad & for \qquad i = 1, .., N \end{aligned} \tag{4.13}$$

Since these constraints are considered in the vehicle's lateral and longitudinal controllers, there is no need to apply them to the optimization problem.

The following constraints are due to the comfort objective. First of all, the vehicle's speed should not exceed a certain amount to ensure the safety and comfort of passengers.

$$V_x(i) \leq \bar{V_x} \qquad for \qquad i = 1, .., N \tag{4.14}$$

In the speed profile design of the vehicle, this constraint is also taken into account, since the speeds of the car cannot be greater than those imposed by law (3.25).

As discussed in section (4.1), the vehicle's lateral and longitudinal acceleration and jerk cannot exceed a certain amount. Optimization takes these constraints into account.(see table 4.2).

The final constraint relates to optimization variables. Three parameters are discussed as optimization variables during control design.f_c, the cut-off frequency in Butterworth filter (3.27), and C the comfort parameter in speed profile design (3.26), and R, the weight on input matrix in lateral control (3.13). The defined objective function is most affected by these three parameters.

In lateral controllers, R plays a crucial role in minimizing lateral error. With small values of R, the path cannot be followed perfectly, especially in parts with high curvatures. In contrast, large values of R result in fluctuations during path-following. Therefore, it is important to select the appropriate range for R.

When designing a speed profile, f_c and C have a crucial impact on smoothness. We know that the smoother the speed the more comfort will be provided to passengers. Having large values of C and f_c results in a small average speed during the whole journey, which increases travel time.

Moreover, the coupling between lateral and longitudinal control should not be overlooked since longitudinal speed affects the lateral model of the vehicle and results in different lateral errors.

Therefore, the final ranges of optimization variables are:

$$\begin{aligned} R &= [100,\ 200] \\ f_c &= [4,\ 12] \\ C &= [10,\ 30] \end{aligned} \tag{4.15}$$

Optimization variables are constrained by these ranges.

4.2.3. Final Formulation

After discussing all the elements in an optimization problem, we can now write the final formulation.

$$\min_{X} \quad J = w_{speed}J_{speed} + w_{comfort}J_{comfort} + w_{lateral}J_{lateral} \tag{4.16a}$$

$$\text{s.t.} \quad \zeta(i+1) = f_{\zeta}(\zeta(i), u(i), \theta, X) \qquad i = 1, ...N \tag{4.16b}$$

$$y(i) = g_{\zeta}(\zeta(i), u(i), \theta, X) \qquad i = 1, ...N \tag{4.16c}$$

$$\underline{j_x} \leq j_x(i) \leq \overline{j_x} \qquad i = 1, ...N \tag{4.16d}$$

$$\underline{j_y} \leq j_y(i) \leq \overline{j_y} \qquad i = 1, ...N \tag{4.16e}$$

$$\underline{a_x} \leq a_x(i) \leq \overline{a_x} \qquad i = 1, ...N \tag{4.16f}$$

$$\underline{a_y} \leq a_y(i) \leq \overline{a_y} \qquad i = 1, ...N \tag{4.16g}$$

$$\underline{f_c} \leq f_c \leq \overline{f_c} \tag{4.16h}$$

$$\underline{C} \leq C \leq \overline{C} \tag{4.16i}$$

$$\underline{R} \leq R \leq \overline{R} \tag{4.16j}$$

Where $X = [f_c, C, R]^T$ is the optimization variable. The Model in the equation (4.16b) and (4.16c) is the non-linear closed-loop driver model of vehicle. The minimum and maximum values of constraints are discussed before and listed in table in (4.3). N refers to the number of waypoints on the path that optimization is applied to. Optimization can be applied to the entire path or to a small part of it which results in a change in the number of waypoints. Furthermore, the number of waypoints varies depending on the length of path.

Variable	Description	Value
$\underline{j_x}$	minimum longitudinal jerk	-0.9 ms^{-3}
$\underline{j_y}$	minimum lateral jerk	-0.9 ms^{-3}
$\underline{a_x}$	minimum longitudinal acceleration	-2 ms^{-2}
$\underline{a_y}$	minimum lateral acceleration	-2 ms^{-2}
$\underline{f_C}$	minimum cut-off frequency of Butterworth filter	$4Hz$
$\underline{C}$	minimum comfort parameter	10
$\underline{R}$	minimum weight input matrix (LQR)	100
$\overline{j_x}$	maximum longitudinal jerk	0.9 ms^{-3}
$\overline{j_y}$	maximum lateral jerk	0.9 ms^{-3}
$\overline{a_x}$	maximum longitudinal acceleration	2 ms^{-2}
$\overline{a_y}$	maximum lateral acceleration	2 ms^{-2}
$\overline{f_c}$	maximum cut-off frequency of Butterworth filter	$12Hz$
$\overline{C}$	maximum comfort parameter	30
$\overline{R}$	maximum weight input matrix (LQR)	200

Table 4.3: Minimum and maximum values of constraints in optimization problem

4.2.4. Optimization Algorithm

Taking into consideration the highly nonlinear nature of the vehicle as well as the control system design, it is a challenging to solve the optimization problem. Grid approach is a simple solution to this problem. The cost function is thus minimized over the feasible set of optimization variables. Within the range of the optimization variables, the sets of variables are further divided into discrete values. Different methods can be used for discretizing a set, such as uniform discretization. This approach results in discrete cost functions. Therefore, in each iterative, the cost function is computed based on the value of optimization variables in the set and then the minimum is found in the end.

$$\begin{aligned} \min_{X} \quad & J(X) \\ \text{s.t.} \quad & X \in D \end{aligned} \tag{4.17}$$

Where D is the collection of feasible arrangements of variables and $J(X)$ measures the the objective value using different combinations of of X.
Here, the optimization variables $X = [f_c,\ C,\ R]$. Where, R is the weighting input matrix

in (3.13), f_c is the cut-off frequency in (3.27), and C is the comfort parameter in (3.26). The process can be summarized as follows:

Algorithm 4.1 Gridding Optimization

1: Consider feasible range of $X \in (\underline{X}, \overline{X})$
2: Division of the selected range into discrete values $(\underline{X}, X_2, .., X_i, .., \overline{X})$
3: Arrangement of different combination of variables (D)
4: Calculate the cost function using different arrangements (J(X))
5: Select the minimum cost function value and corresponding optimization variable values

In this study, step 1) The feasible range of the optimization variables are defined in (4.15). Step 2) These ranges are discritized into four values as follows:

$$\begin{aligned} R &= [100, 125, 150, 200] \\ f_c &= [4, 6, 10, 12] \\ C &= [10, 15, 25, 30] \end{aligned} \tag{4.18}$$

Moreover, the combination of these vectors results in the arrangement vector (D) with a size of 64. Step 3) each arrangement is then used to calculate the cost function. Finally, the minimum cost function and the arrangement that results in the minimum cost function is selected.

Two plots of level curves is shown in here. first in figure (4.1), R is constant and equal to 125. Then, f_c and C change within the range. In addition, a second curve (4.2) is made by setting the f_c constant to 4 and changing R and C within the range. The cost functions in these level curves are not normalized, and all objective functions have weights of 1.

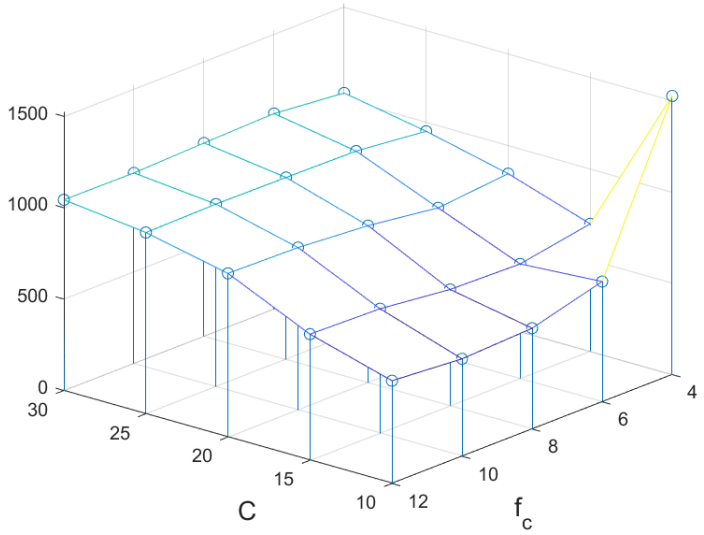

Figure 4.1: Level curve of cost function with different arrangements of f_c and C. R is constant.

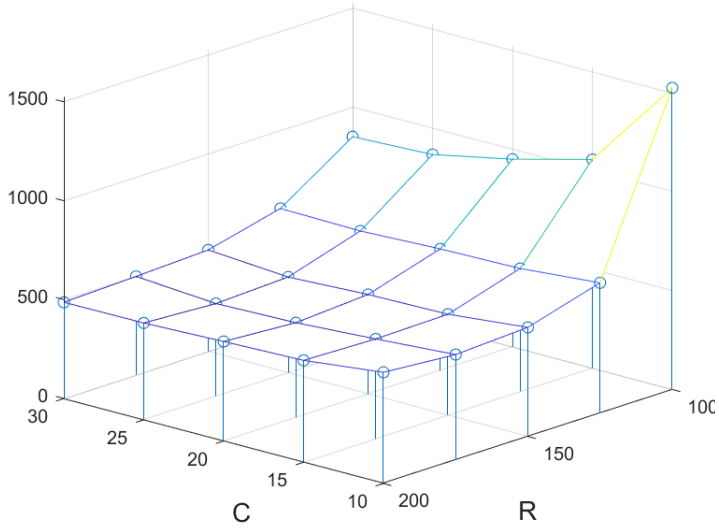

Figure 4.2: Level curve of cost function with different arrangements of R and C. f_c is constant.

4.3. Multi-Objective Optimization

The concept of multi-objective optimization (MOO) refers to the optimization of problems that have more than one objective function that needs to be minimized or maximized. In order to solve these problems, we need a set of solutions that balance objectives in the best way possible. In single objective problems, the superiority of one solution over another can be easily computed by comparing the cost functions. A multi-objective optimization solution, however, is the one that dominates all others. Multi-objective problems can be solved in different ways, such as Goal attainment, Minmax, and Pareto front. Pareto front identifies solutions in which advancement in one objective requires a compromise in another. These solutions are also referred to as non-dominant solutions. A non-dominated set of solutions refers to those solutions that are not dominated by any other solution in the set. The non-dominated set is called the Pareto optimal set, and the boundary defined by mapping all the solutions in the set is called the Pareto optimal front.

There is a conflict between all the cost functions defined in this study. Travel time and lateral error increase when comfort is maximized. Minimizing lateral error results in longer travel time and vice versa.

Multi-objective optimization is done on the path in the figure (4.3). Here's the real-world path exported from OpenStreetMap to Driving Scenario Designer. Path is chosen to have high curves rates and tangent angles, so comfort, lateral, and speed cost functions are challenged (see figure 4.5).

Nevertheless, the length of the road makes the optimization computation time very long, so only a small part of the path is considered for analysis (see figure 4.4). A coordinate change is also applied to the real path so that the starting point becomes $X_0 = 0, Y_0 = 0$. The center line of the road is chosen as the reference path for vehicle.

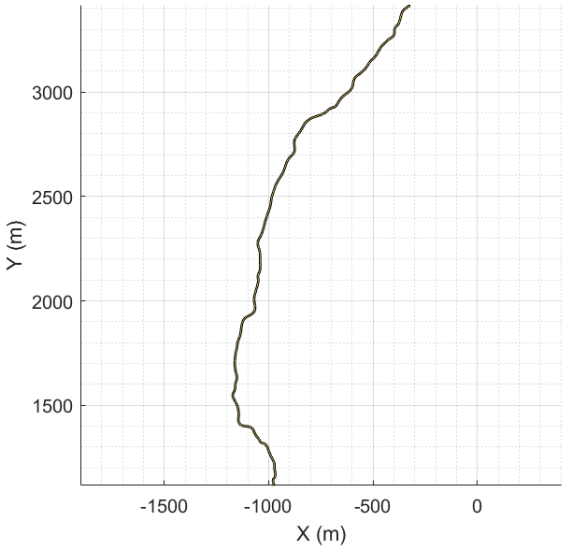

Figure 4.3: The road used for multi-objective analysis. The width of the road is 6 m.

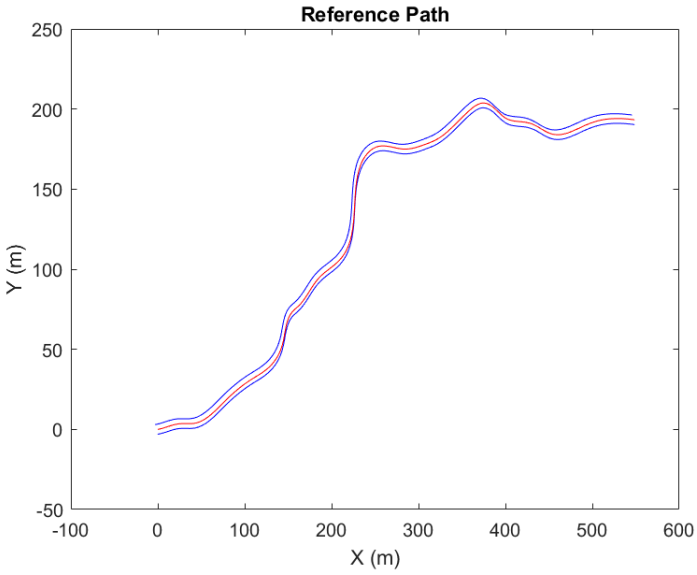

Figure 4.4: The part of the road that is selected for multi-objective analysis. The total of the path is 639 (m), and (0,0) is the starting point. The blue lines are the borders of the road and the red line is the center line of the road The width of the road is 6 m.

The following diagram shows how the reference path's curvature and tangent angle change over distance.

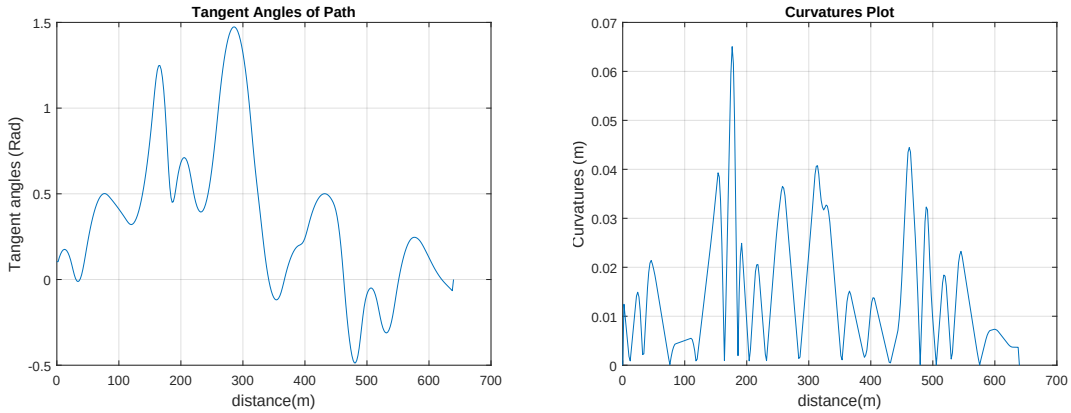

(a) Tangent angles of the path over distance. (b) Curvatures of the path over distance.

Figure 4.5: Reference path features used for multi-objective analysis

Optimizing weighted sums is one way to solve the multi-objective problem. This method optimizes the weighted sum of cost functions by choosing positive scalars as weights of each cost function.

In order to build a Pareto front, different tests (table 4.4) are conducted. In each test, the aim is to find the minimum objective function. As a result, in each test, the arrangement of optimization variables that makes the objective function minimum is chosen. In other words, for each combination of weights, optimization of control parameters is repeated. Then, using the arrangement of optimization variables (control parameters), resulting in the minimum cost function is chosen. Then lateral error, speed, accelerations, and jerks during path-following are measured using this arrangement. After that, these data are used to build different Pareto fronts.

Accordingly, to build the Pareto front in this study, w_{speed}, $w_{comfort}$, $w_{lateral}$, as introduced in objective function in (4.16a), is chosen as follows. In the first place, w_{speed} is chosen as a constant. $w_{comfort}$ and $w_{lateral}$ are changing in opposite pattern.

	w_{speed}	$w_{comfort}$	$w_{lateral}$
Test 1	1	20	0.2
Test 2	1	7	3
Test 3	1	5	5
Test 4	1	3	7
Test 5	1	1	10
Test 6	1	0.2	20

Table 4.4: Different tests to obtain Pareto front

Which means while $w_{comfort}$ is decreasing, $w_{lateral}$ is increasing. After carrying out 6 tests with different weights, the Pareto front is calculated taking into account the lateral cost function as well as the comfort cost function.

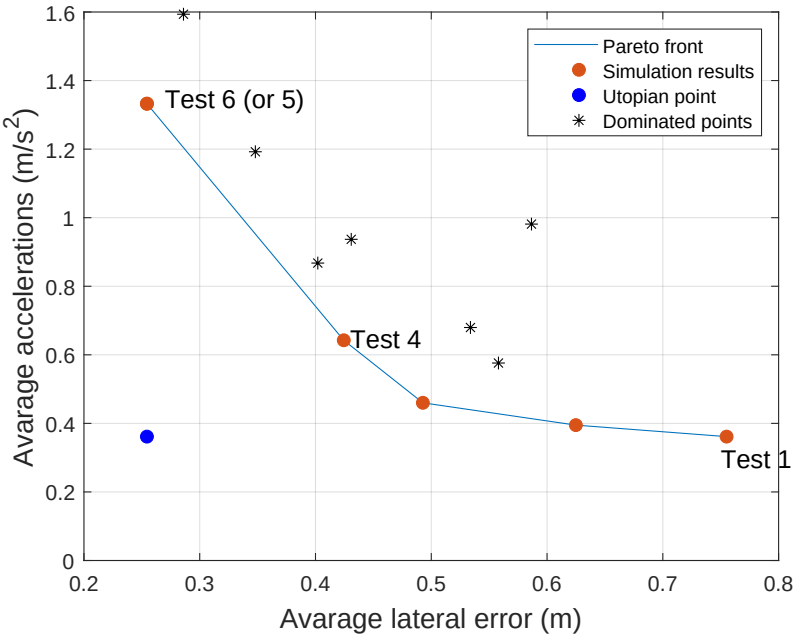

Figure 4.6: Pareto front with average lateral error during path-following and average accelerations.

An average lateral error during the path is compared with an average of longitudinal and lateral accelerations to form the Pareto front (see figure 4.6). The results of test 5 and test 6 are the same on the Pareto front. It can be seen that the Pareto front is close to

the Utopian point when Test 3 or Test 4 is carried out where ($w_{comfort} = w_{lateral} = 5$) and ($w_{comfort} = 3, w_{lateral} = 7$) respectively. In addition, a few points which are dominated by the Pareto front are shown in the figure (4.6). As predicted, the lateral error is the highest when comfort is at its lowest value. However, the average of accelerations may not be a proper representation of comfort. Thus, The Pareto front built in figure (4.6) is represented in another way. Here, the maximum of lateral error during path-following is compared to the Illness Rating (IR) (see figure 4.7).

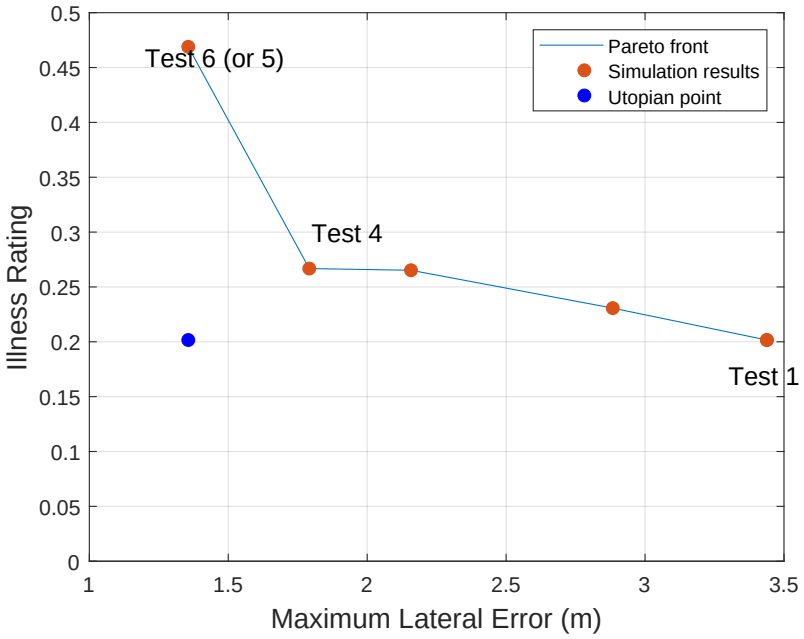

Figure 4.7: Representation of Pareto front with maximum lateral error during path-following and illness rating (IR).

It should be remembered that the Pareto front in figure (4.7) is another representation of the Pareto front in figure (4.6). So the Pareto front is built based on average lateral error and average accelerations, but it's presented in this manner to better reflect comfort. However, after following the whole path, the illness rating (IR) is lower than 1 in all the tests which means passengers are comfortable in all tests. (based on table 4.1).

Furthermore, the Pareto front is performed for speed and comfort cost functions which can be found in Appendix B.

Weights can be chosen based on our goals. If the weights are $w_{lateral} = 0.2, w_{comfort} = 20, w_{speed} = 1$, comfort is at its best level, whereas lateral error is at its maximum. In contrast, when $w_{lateral} = 20, w_{comfort} = 0.2, w_{speed} = 1$, the lateral error is minimum,

but the comfort of the passengers is worst. If we want to consider the lateral error cost function and passenger comfort level equally, the closest point to the Utopian point on the Pareto front should be chosen where $w_{lateral} = 5, w_{comfort} = 5, w_{speed} = 1$ or $w_{comfort} = 3, w_{lateral} = 7, w_{speed} = 1$.

In the following figure (4.8), you can see how the control parameters change from test to test. For example, for test 1 where the comfort is at its highest, the value control parameters are $f_c = 4, C = 10, R = 200$. For test 6 (or 5) with a smallest lateral error, the value of control parameters are $f_c = 12, C = 30, R = 125$.

Further, there is a coupling between the lateral and longitudinal control of the vehicle. For example, longitudinal velocity also affects the lateral model of the controller and the vehicle. Therefore, f_c and C are parameters in the longitudinal controller but they also impact lateral error.

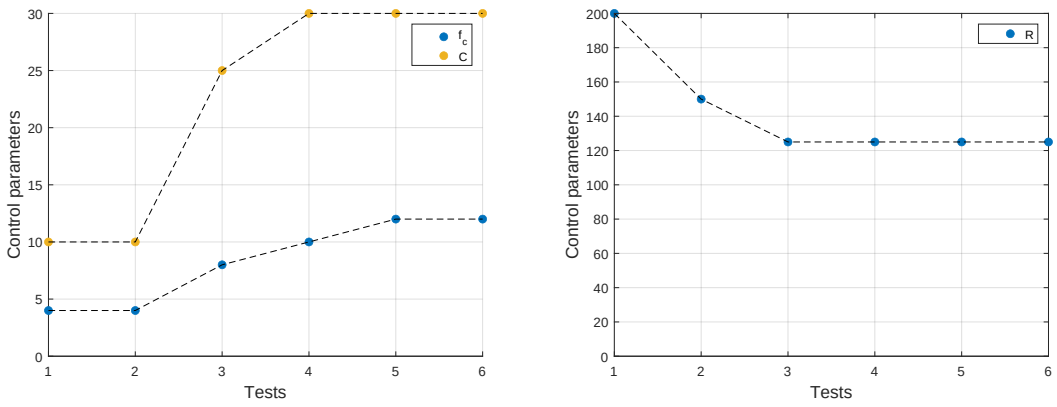

(a) f_c and C (b) R

Figure 4.8: Optimal control parameters for each test. f_c is cut-off frequency in Butterworth filter, C is the comfort parameter in reference speed generation and R is the weighting input matrix in LQR control.

In order to choose the appropriate weighting, the Pareto front of comfort and speed cost functions is also considered (Appandix B). Since the prior goal of this thesis was to provide comfort for passengers as they followed the predefined path, the Pareto front of lateral error and speed cost function is not a subject of this thesis.

A spider diagram can also be used to visualize the cost function values by different weights.

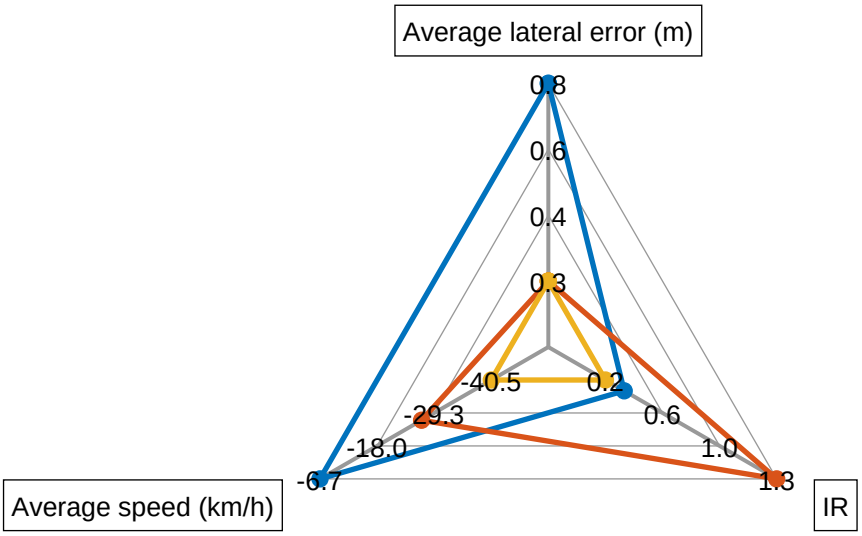

Figure 4.9: Spider diagram showing the Utopian point(yellow line), and the Pareto optimal solution obtained by $w_{lateral} = 20, w_{comfort} = 0.2, w_{speed} = 1$ (red line), and $w_{lateral} = 0.2, w_{comfort} = 20, w_{speed} = 1$ (blue line). The minus of average speed is shown in figure because the goal is to maximize the speed in thesis.

Finally, The weight of objective functions for optimization problem are chosen $w_{lateral} = 3, w_{comfort} = 7, w_{speed} = 3$ which is the closet point on Pareto front to Utopian point in figure (4.6 and B.1).

Based on these weights, The optimization again carried out and The optimal control parameters are:

$$\begin{aligned} f_c &= 6 \\ R &= 200 \\ C &= 20 \end{aligned} \tag{4.19}$$

4.4. Performance Evaluation

The designed controllers using the optimized parameters are applied to the following path in order to verify the results. The road is chosen from an area in northern Italy close to Aosta. The total distance of the path is 743.6m and 373 waypoints with the distance of 2m on the path are chosen.

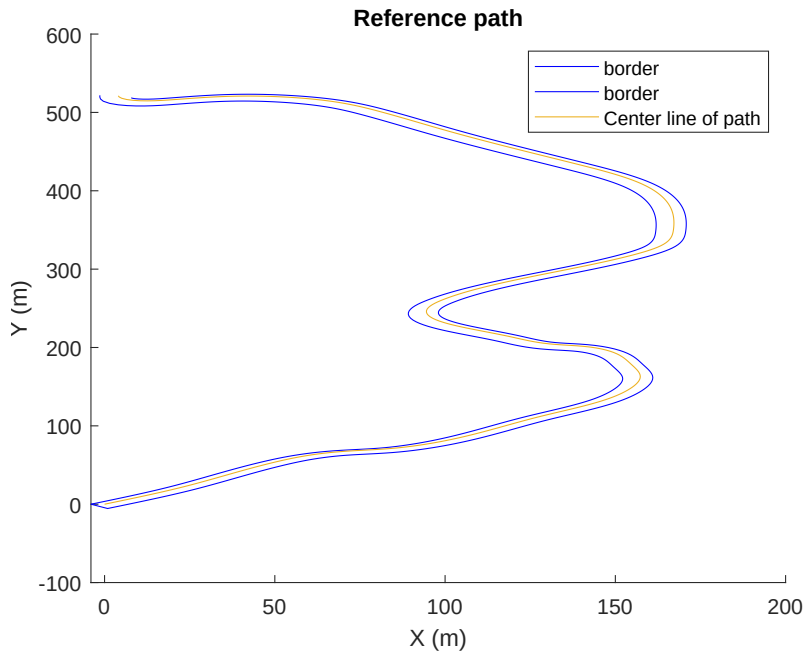

Figure 4.10: Road in the global coordinate. The starting point of the center line of the path is $(0, 0)$.

In the path-following model, the center line of the road is used as the reference path. As a result, all the characteristics of the road's center line are extracted. A change in coordinates is also applied to the path.

The center line of the road has the below characteristics:

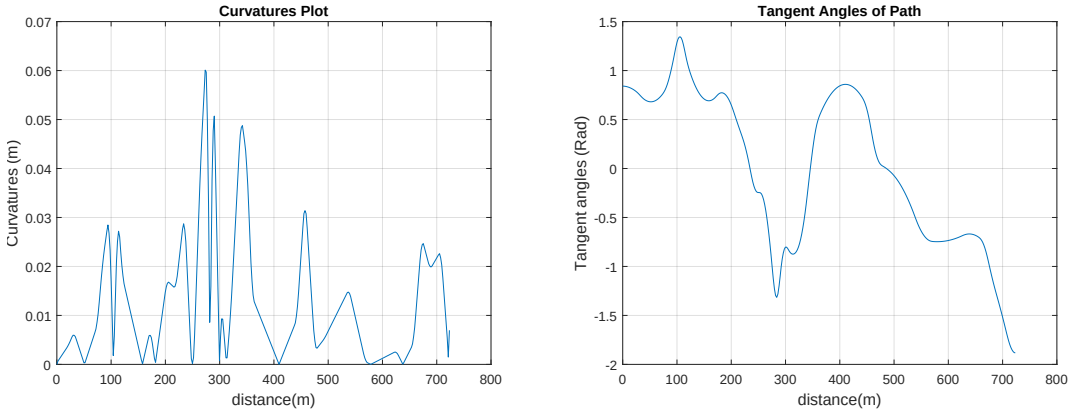

(a) Curvatures of the path over distance. (b) Tangent angles of the path over distance.

Figure 4.11: Reference path features used performance evaluation

Following the application of the driver model on reference path, we obtain the following results.
The vehicle follows the reference path as can be seen from the image below (4.12). During many parts of the journey there is no lateral error between the vehicle and the path. However, in some parts, the lateral error is much greater, with a maximum error of 1.47 m. The vehicle, however, remains within the road's border. The average of lateral error during the whole path is 0.36 m.

Then the speed profile is shown in figure (4.13). In longitudinal control, the reference speed is the speed designed by the speed profile designer, and then cruise control ensures that the vehicle follows the reference speed accurately and efficiently.

Finally, the longitudinal and lateral jerks and acceleration of the vehicle are measured. As can be seen in the figure (4.14), they remain within the thresholds except for the time when the vehicle starts following the path for the first time. This is due to the initialization of the controller parameters which makes the model unstable initially.
In addition, the illness rating (IR) based on the equation (4.7) is calculated and it is:

$$IR = 0.405 \tag{4.20}$$

Therefore, considering the table (4.1) , it is lower than 1 which results in comfort of passengers.

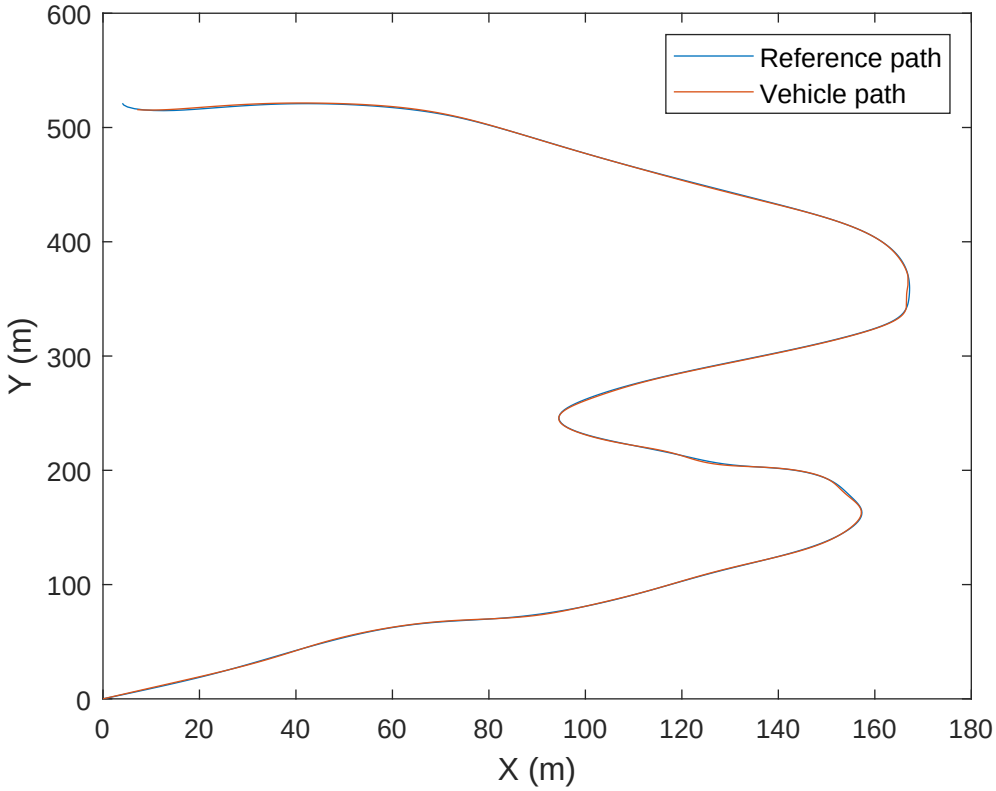

Figure 4.12: Path-following result

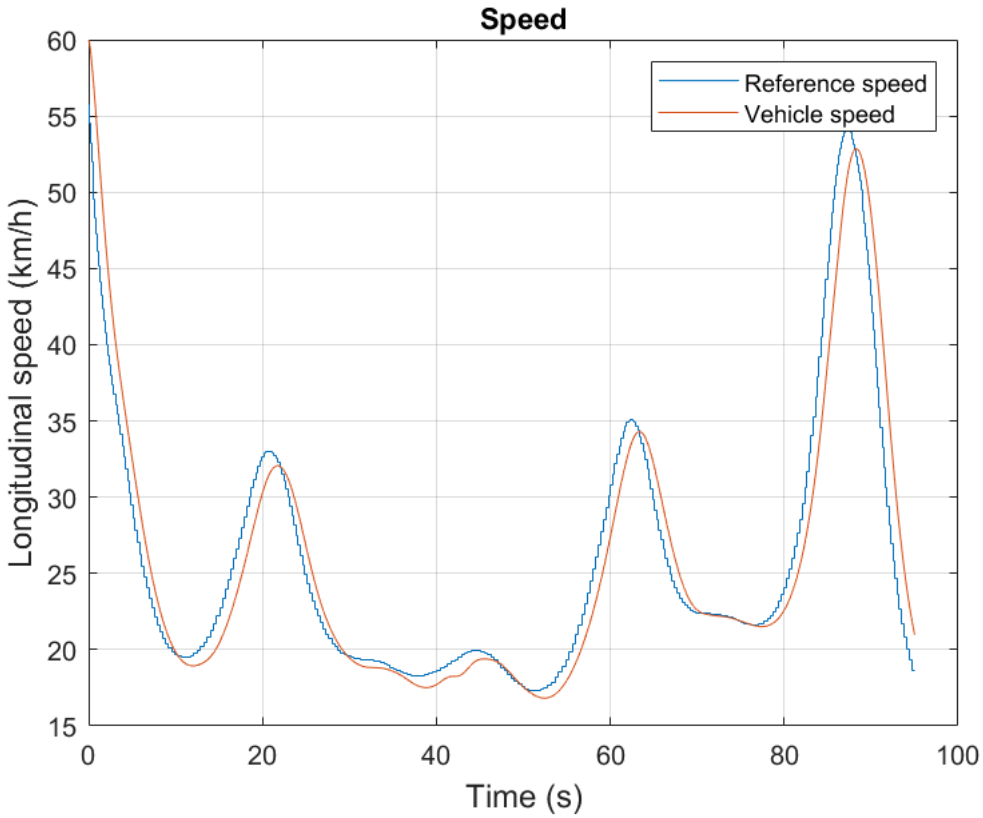

Figure 4.13: The reference speed and the vehicle's speed

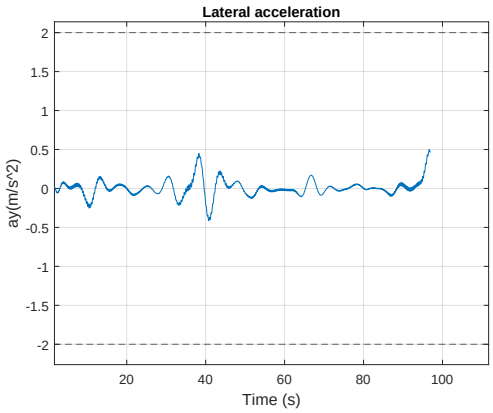

(a) Lateral acceleration of vehicle while following the path.

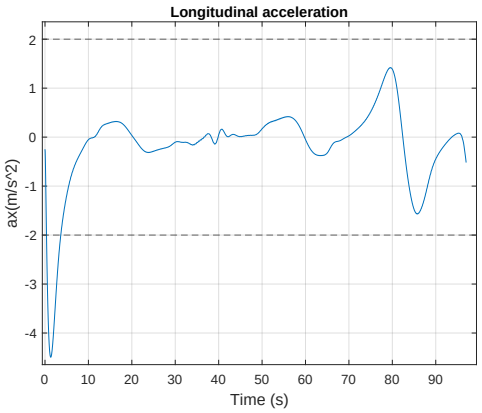

(b) Longitudinal acceleration of vehicle while following the path

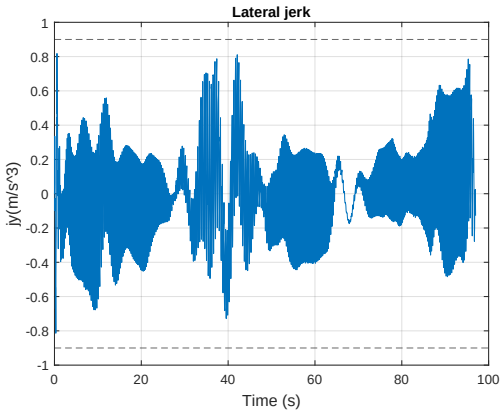

(c) Lateral jerk of vehicle while following the path

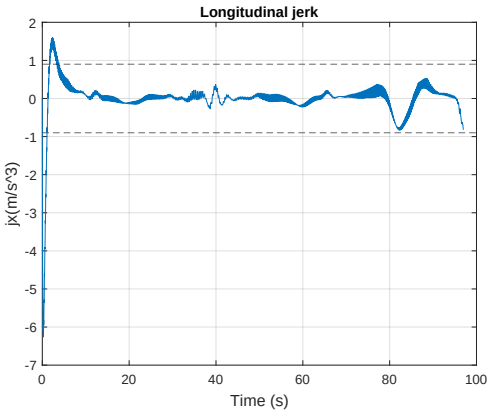

(d) Lateral jerk of vehicle while following the path

Figure 4.14: Accelerations and jerks of the vehicle during path-following

5 | Conclusions and Future Developments

5.1. Conclusions

This thesis aims to design longitudinal and lateral controllers for autonomous vehicles so that they can follow a path while providing comfort for passengers and reducing travel time to the maximum extent possible in the process. Additionally, keep the vehicle as close to the center line of the road as possible.

We have taken into account different path-following methods from the literature. Most algorithms in path following aim to keep the vehicle on the road without considering the comfort of passengers or the travel time. Additionally, the majority of path following algorithms ignore the dynamics of the vehicle and rely on geometric relationships between path and vehicle, which may lead to poor results at high speeds or emergency situations. This study developed a path-following model based on a dynamic model of a vehicle along with considering the comfort of its passengers and travel time.

This study models the path using waypoints. As a result of using waypoints to model the path, the problem is independent of time. In the optimization phase, the problem is easier since it is independent of time.

In this thesis, the multi-point preview method is also considered for modeling the relation between driver and path during path-following. In many path following methods, only one preview point is taken into account, which is unrealistic and can result in poor path-following. Since one point is not sufficient to model the road in front of the driver.

To develop a driver model for vehicles, both a nonlinear and a linear bicycle model are considered. Both lateral and longitudinal control are included in the driver model. Additionally, the vehicle's inputs are its steering angle and torque. First, a lateral controller for the vehicle is developed. The lateral controller is a cascade controller in which the outer loop produces the desired yaw rate as a reference for the inner loop, which controls

the vehicle's yaw. Linear Quadratic Regulator (LQR) is used to design the outer loop, and PI controllers are used for the inner loop. During design, it was also considered that the inner loop should be at least ten times faster than the outer loop.

Two parts make up the longitudinal controller. Initially, a speed profile designer is employed. The speed is determined by the curvature of the path. The smooth speed of a vehicle is a key factor in passenger comfort. Therefore, a low pass filter is applied to a reference speed to make it smoother. In order for the vehicle to follow the reference speed, the cruise control is used. Using PI controllers, this controller has been designed.

It can be said that the three objective functions that are correlated with discomfort, travel time, and lateral deviation of the vehicle from the path act against one another. The goal of this study is to determine some parameters of the closed-loop system model that optimize the above mentioned objective functions at the best possible value. We chose the parameters that have the greatest impact on our objective, namely the cut-off frequency in the low-pass filter, the comfort parameter in the speed profile design, and input weight matrix (R) in the path-following lateral control. The problem is solved using a multi-objective optimization technique. Based on Pareto front, the weights of the objectives are adjusted.

Then, different real-world paths are extracted from OpenStreetMap and tested. The vehicle follows the paths while adhering to comfort criteria and staying within the road's boundaries.

According to the research, it has been demonstrated that with proper design of the lateral and longitudinal control system, autonomous vehicles are capable of following predefined roads while providing comfort to passengers and reducing travel time. There is no doubt that autonomous vehicles can be more trustworthy for drivers and passengers due to the fact that comfort and safety are the most significant factors for passengers while they are driving.

5.2. Future Developments

This thesis considers static environments with predefined paths. Consequently, if an obstacle enters the path, the vehicle cannot handle it. Therefore, one of the future tasks could be to develop a trajectory following system that takes into account moving obstacles while considering the dynamic environment. Another vehicle on the road can be one of these moving obstacles. So, lateral controllers can adjust the steering angle so as to avoid colliding with the leading car, and longitudinal controllers can design the reference speed based on the lead car to maintain the distance with it.

In addition, in outer loop of lateral cascade controller there are disturbances due to the lateral and longitudinal velocity of vehicle . These disturbances are rejected in the inner loop of the cascade controller. Nevertheless, Due to the fact that the diturbacnes are known and can be estimated, a feed forward controller can be designed in lateral part to take into account these disturbances.

The optimization variables are discretized into four values to shorten the computation time of the optimization. They can be discretized into more numbers to find a better solution if one exists.

Gridding strategy is used to optimize the closed-loop system due to its non-linearity. However, other optimization algorithms suitable for nonlinear systems such as Sequential Quadratic Programming (SQP) can be applied to the closed-loop system as well.

Bibliography

[1] . Are Mjaavatten (2022). Curvature of a 1D curve in a 2D or 3D space (https://www.mathworks.com/matlabcentral/fileexchange/69452-curvature-of-a-1d-curve-in-a-2d-or-3d-space), MATLAB Central File Exchange. Retrieved November 8, 2022.

[2] . Lorenzo Fagiano and Marco Lauricella. Laboratory session A - Simulation of continuous time, nonlinear dynamical systems' models. Constrained Numerical Optimization for Estimation and Control Course.

[3] A. F. Abercromby, W. E. Amonette, C. S. Layne, B. K. McFarlin, M. R. Hinman, and W. H. Paloski. Vibration exposure and biodynamic responses during whole-body vibration training. *Medicine and science in sports and exercise*, 39(10):1794, 2007.

[4] O. Amidi. Integrated mobile robot control. Technical Report CMU-RI-TR-90-17, Carnegie Mellon University, Pittsburgh, PA, May 1990.

[5] M. Canale, L. Fagiano, M. Milanese, and P. Borodani. Robust vehicle yaw control using an active differential and imc techniques. *Control Engineering Practice*, 15(8): 923–941, 2007.

[6] C. Certosini, R. Capitani, and C. Annicchiarico. Optimal speed profile on a given road for motion sickness reduction. *arXiv preprint arXiv:2010.05701*, 2020.

[7] C. Corbridge. *Vibration in vehicles: its effect on comfort*. PhD thesis, University of Southampton, 1987. URL `https://eprints.soton.ac.uk/52265/`.

[8] M. G. Da Silva. Measurements of comfort in vehicles. *Measurement Science and Technology*, 13(6):R41, 2002.

[9] A. El Hajjaji and S. Bentalba. Fuzzy path tracking control for automatic steering of vehicles. *Robotics and Autonomous systems*, 43(4):203–213, 2003.

[10] M. Elbanhawi, M. Simic, and R. Jazar. In the passenger seat: investigating ride comfort measures in autonomous cars. *IEEE Intelligent transportation systems magazine*, 7(3):4–17, 2015.

[11] D. J. Fagnant and K. Kockelman. Preparing a nation for autonomous vehicles: opportunities, barriers and policy recommendations. *Transportation Research Part A: Policy and Practice*, 77:167–181, 2015.

[12] B. D. Graaf and W. Van Weperen. The retention of blance: An exploratory study into the limits of acceleration the human body can withstand without losing equilibrium. *Human factors*, 39(1):111–118, 1997.

[13] M. J. Griffin and J. Erdreich. Handbook of human vibration, 1991.

[14] I. ISO. 2631-1: Mechanical vibration and shock-evaluation of human exposure to whole-body vibration-part 1: General requirements. *Geneva, Switzerland: ISO*, 1997.

[15] K. Jalali, S. Lambert, and J. McPhee. Development of a path-following and a speed control driver model for an electric vehicle. 2012.

[16] M. Lalo and R. Scattolini. *Advanced and multivariable control.* Pitagoga edirice Bologna, 2014.

[17] A. Lawther and M. J. Griffin. Prediction of the incidence of motion sickness from the magnitude, frequency, and duration of vertical oscillation. *The Journal of the Acoustical Society of America*, 82(3):957–966, 1987.

[18] W. H. Levison, A. C. Bittner Jr, J. L. Campbell, and C. Schreiner. Modification and partial validation of the driver/vehicle module. *Transportation research record*, 1803 (1):52–58, 2002.

[19] Y. Liang, Y. Li, L. Zheng, Y. Yu, and Y. Ren. Yaw rate tracking-based path-following control for four-wheel independent driving and four-wheel independent steering autonomous vehicles considering the coordination with dynamics stability. *Proceedings of the Institution of Mechanical Engineers, Part D: Journal of Automobile Engineering*, 235(1):260–272, 2021.

[20] C. Liu, W. Zhan, and M. Tomizuka. Speed profile planning in dynamic environments via temporal optimization. In *2017 IEEE Intelligent Vehicles Symposium (IV)*, pages 154–159. IEEE, 2017.

[21] A. D. Luca, G. Oriolo, and C. Samson. Feedback control of a nonholonomic car-like robot. *Robot motion planning and control*, pages 171–253, 1998.

[22] J. A. Matute, M. Marcano, A. Zubizarreta, and J. Perez. Longitudinal model predictive control with comfortable speed planner. In *2018 IEEE International Conference*

on Autonomous Robot Systems and Competitions (ICARSC), pages 60–64. IEEE, 2018.

[23] M. E. McCauley, J. W. Royal, C. D. Wylie, J. F. O'Hanlon, and R. R. Mackie. Motion sickness incidence: Exploratory studies of habituation, pitch and roll, and the refinement of a mathematical model. Technical report, Canyon Research Group Inc Goleta Ca Human Factors Research Div, 1976.

[24] W. F. Milliken, D. L. Milliken, and L. D. Metz. *Race car vehicle dynamics*, volume 400. SAE international Warrendale, 1995.

[25] F. Mohseni, J. Åslund, E. Frisk, and L. Nielsen. Fuel and comfort efficient cooperative control for autonomous vehicles. In *2017 IEEE intelligent vehicles symposium (IV)*, pages 1631–1636. IEEE, 2017.

[26] S. Moon and K. Yi. Human driving data-based design of a vehicle adaptive cruise control algorithm. *Vehicle System Dynamics*, 46(8):661–690, 2008.

[27] A. Ollero and G. Heredia. Stability analysis of mobile robot path tracking. In *Proceedings 1995 IEEE/RSJ International Conference on Intelligent Robots and Systems. Human Robot Interaction and Cooperative Robots*, volume 3, pages 461–466 vol.3, 1995. doi: 10.1109/IROS.1995.525925.

[28] D. Paddeu, G. Parkhurst, and I. Shergold. Passenger comfort and trust on first-time use of a shared autonomous shuttle vehicle. *Transportation Research Part C: Emerging Technologies*, 115:102604, 2020.

[29] R. Rajamani. *Vehicle dynamics and control*. Springer Science & Business Media, 2011.

[30] P. Ritzer, C. Winter, and J. Brembeck. Advanced path following control of an overactuated robotic vehicle. In *2015 IEEE Intelligent Vehicles Symposium (IV)*, pages 1120–1125. IEEE, 2015.

[31] M. Sivak and B. Schoettle. Motion sickness in self-driving vehicles. Technical report, University of Michigan, Ann Arbor, Transportation Research Institute, 2015.

[32] S. Thrun, M. Montemerlo, H. Dahlkamp, D. Stavens, A. Aron, J. Diebel, P. Fong, J. Gale, M. Halpenny, G. Hoffmann, K. Lau, C. Oakley, M. Palatucci, V. Pratt, P. Stang, S. Strohband, C. Dupont, L.-E. Jendrossek, C. Koelen, C. Markey, C. Rummel, J. van Niekerk, E. Jensen, P. Alessandrini, G. Bradski, B. Davies, S. Ettinger, A. Kaehler, A. Nefian, and P. Mahoney. Winning the darpa grand challenge. *Journal of Field Robotics*, 2006. accepted for publication.

[33] Y. Wang, J.-R. Chardonnet, and F. Merienne. Speed profile optimization for enhanced passenger comfort: An optimal control approach. In *2018 21st International Conference on Intelligent Transportation Systems (ITSC)*, pages 723–728. IEEE, 2018.

[34] J. Zhou, R. He, Y. Wang, S. Jiang, Z. Zhu, J. Hu, J. Miao, and Q. Luo. Autonomous driving trajectory optimization with dual-loop iterative anchoring path smoothing and piecewise-jerk speed optimization. *IEEE Robotics and Automation Letters*, 6(2): 439–446, 2021. doi: 10.1109/LRA.2020.3045925.

A | Appendix A

In the table below, you will find the values for the parameters of the vehicle model in Simulation. The values are from [5].

Variable	Description	Value
$\boldsymbol{m}$	Vehicle mass	1715 Kg
$\boldsymbol{J_z}$	Vehicle moment of inertia	2700 kg m^2
$\boldsymbol{a}$	Distance between COG and front axle	1.07 m
$\boldsymbol{b}$	Distance between COG and rear axle	1.47 m
$\boldsymbol{C_f}$	Front cornering stiffness	95117 $Nrad^{-1}$
$\boldsymbol{C_r}$	Rear cornering stiffness	97556 $Nrad^{-1}$
$\boldsymbol{r_w}$	Wheel radius	0.303 m
$\boldsymbol{\mu}$	Road-tire friction coefficient	1
$\boldsymbol{A_f}$	Vehicle front area	1.9 m^2
$\boldsymbol{A_l}$	Vehicle lateral area	3.2 m^2
$\boldsymbol{C_x}$	Vehicle front aerodynamic drag coeff	0.4
$\boldsymbol{R_r}$	Total rolling resistance	8.97 N s m^{-1}
$\boldsymbol{\rho}$	Air density	1.2 kgm^{-3}
$\bar{\boldsymbol{\delta}}$	Front steering angle limits	0.61 rad
$\boldsymbol{T_{d,max}}$	Maximum traction torque	890 Nm
$\boldsymbol{T_{d,min}}$	Minimum braking torque	-5100 Nm

Table A.1: Parameter values of vehicle used in Simulation

Normalised Low Pass Butterworth Filter Polynomials corresponding to the cut-off frequency 1 rad/s. n is the order of the filter.

n	Denominator
1	$1 + s$
2	$1 + 1.414s + s^2$
3	$(1 + s)(1 + s + s^2)$
4	$(1 + 0.765s + s^2)(1 + 1.848s + s^2)$
5	$(1 + s)(1 + 0.618s + s^2)(1 + 1.618s + s^2)$

Table A.2: Normalised Low Pass Butterworth Filter Polynomials

These polynomials can be computed by butter function in MATLAB.

B | Appendix B

To obtain the Pareto front for speed-comfort objectives, four tests were conducted.

	w_{speed}	$w_{comfort}$	$w_{lateral}$
Test 1	1	10	0.01
Test 2	3	7	0.01
Test 3	5	5	0.01
Test 4	20	0.5	0.01

Table B.1: Different tests to obtain Pareto front

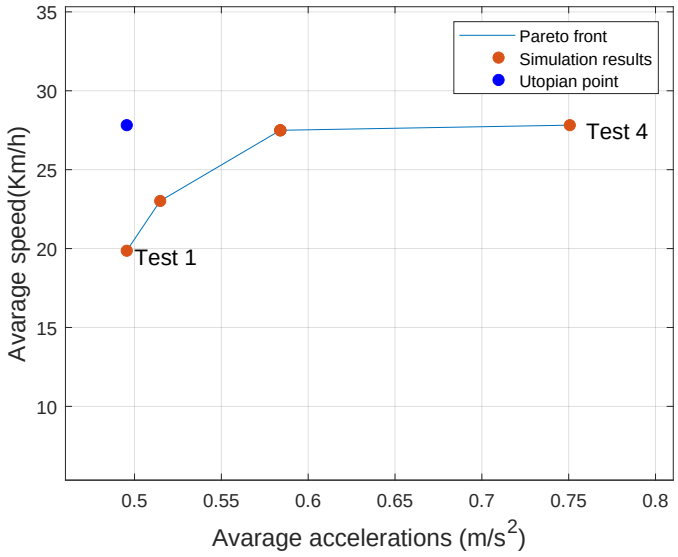

Figure B.1: The Pareto front considering average of acceleration as a sign of comfort and average of speed during path-following

The lower the average acceleration, the more comfortable the passengers will be, and vice

versa. Additionally, a higher average speed means a shorter travel time.
The control parameters changes in following manner for each test.

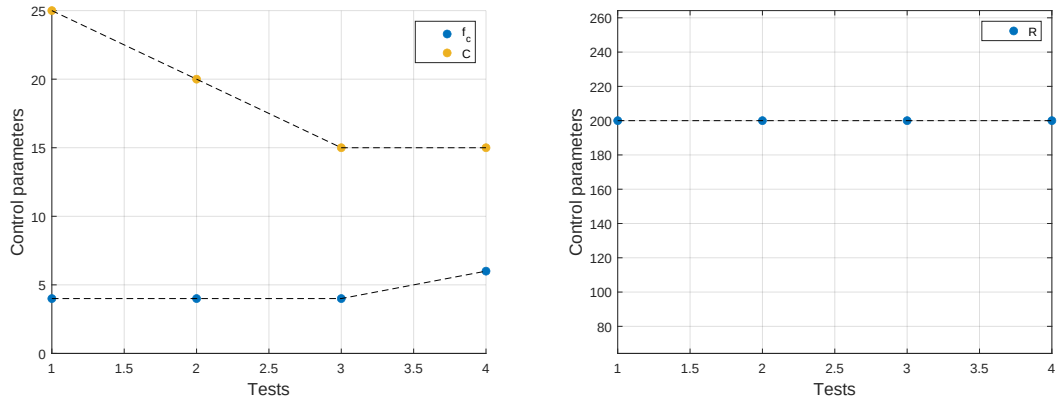

(a) f_c *and* C (b) R

Figure B.2: Optimal control parameters for each test. f_c is cut-off frequency in Butterworth filter, C is the comfort parameter in reference speed generation and R is the weighting input matrix in LQR control.

List of Figures

List of Tables

List of Symbols

Variable	Description	SI unit
$\boldsymbol{\delta}$	Steering angle	Rad
$\boldsymbol{d_{lookahead}}$	Look ahead distance of the car	m
$\boldsymbol{V_x}$	Longitudinal velocity	Kmh^{-1}
$\boldsymbol{V_y}$	Lateral velocity	Kmh^{-1}
$\boldsymbol{a_v}$	vertical acceleration	ms^{-2}
$\boldsymbol{a_x}$	Longitudinal acceleration	ms^{-2}
$\boldsymbol{a_y}$	Lateral acceleration	ms^{-2}
$\boldsymbol{X}$	Longitudinal positions of vehicle	m
$\boldsymbol{Y}$	Lateral positions of vehicle	m
$\boldsymbol{\psi}$	Yaw angle of vehicle	Rad
$\boldsymbol{\beta}$	side slip angle of vehicle	Rad
$\boldsymbol{r}$	yaw rate of vehicle	Rads^{-1}
$\boldsymbol{F_y^f}$	Lateral force of front tire	N
$\boldsymbol{F_y^r}$	Lateral force of rear tire	N
$\boldsymbol{\mu}$	tire-road friction coefficient	
$\boldsymbol{F_z^r}$	rear normal tire load	N
$\boldsymbol{F_z^f}$	front normal tire load	N
$\boldsymbol{T_d}$	traction Torque	Nm
$\boldsymbol{T_{driver}}$	Driver reaction time	s
$\boldsymbol{\Delta\psi}$	yaw angle error	Rad
$\boldsymbol{e_y}$	Lateral error	m
$\boldsymbol{\kappa}$	curvature of path	m
$\boldsymbol{\mu_y}$	lateral tyre-road friction	
$\boldsymbol{H_0}$	maximum passband gain of Buterworth filter	
$\boldsymbol{H_1}$	minimum passband gain of Buterworth filter	
$\boldsymbol{j_x}$	Longitudinal jerk	ms^{-3}
$\boldsymbol{j_y}$	Lateral jerk	ms^{-3}
$\boldsymbol{a_{y.max}}$	Maximum lateral acceleration of vehicle	ms^{-2}

Acronyms	Description
PI	Proprietorial-Integral Controller
LQR	Linear Quadratic Regulator
IR	Illness Rating
MSDV	Motion Sickness Dose Value

Table B.2: Minimum and maximum values of constraints in optimization problem

Acknowledgements

First of all I would like to thank my advisor Professor Lorenzo Fagiano for his valuable feedback and guidance throughout this project. Without his help, the research wouldn't be possible.

The most meaningful thing for me is to thank my family for always supporting me. While they couldn't physically be with me during this journey, they always sent me their love and support.

Furthermore, I would like to thank my friends here who made this path more comfortable for me. The ones who never left my side during tough times and always cared about me. Their kindness will never be forgotten by me.

And lastly, In recent months, Iranians have protested against the oppression and cruelty of the Islamic Regime and fought for their rights. My inspiration comes from Iranian women's bravery every day, and I strive to be as strong as they are. The Islamic regime tortured and murdered over 400 people including children and teenagers. It took me a long time to process the news of one of the victims, Nika Shakarami, a 16-year-old girl whose dead body was discovered by her family after 10 days. A part of me aches when I think about what happened to her during those days. At the end of the day, I wish everyone had a better world to live in.